Geochemical Testing Program for the Cape Coral Aquifer Storage and Recovery System Pilot

FINAL REPORT

Submitted to
City of Cape Coral

By

Cindy Fischler, Paul Hansard, Stuart B. Norton and Jonathan D. Arthur

Florida Department of Environmental Protection, Florida Geological Survey
Tallahassee, Florida

April 15, 2010

Table of Contents

LIST OF FIGURES

LIST OF TABLES

LIST OF APPENDICES

ABBREVIATIONS AND ACRONYMS

Ag	Silver
AgCl	Silver Chloride
Al	Aluminum
Al_2O_3	Aluminum oxide
As	Arsenic
ASR	Aquifer Storage and Recovery
Au	Gold
Ba	Barium
BDL	Below detection limit
Be	Beryllium
Bi	Bismuth
BLS	Below land surface
Br	Bromine
BSE	Backscatter electron
C	Carbon
°C	Degrees Centigrade
C/Co	Leachate concentration / original water concentration
Ca	Calcium
CaO	Calcium Oxide
Cd	Cadmium
Ce	Cerium
CERP	Comprehensive Everglades Restoration Plan
cm	Centimeters
Co	Cobalt
CO_2	Carbon dioxide
CO_3	Carbonate
CPS	Canal Pump Station
Cr	Chromium
Cs	Cesium
Cu	Copper
Coul	Coulometry
DDI	Distilled de-ionized water
DL	Detection limit
DO	Dissolved oxygen
Dy	Dysporium
EC	Electrical conductance
EDS	Energy-dispersive Spectrometer
Eh	Theoretical oxidation-reduction potential
Er	Erbium

ABBREVIATIONS AND ACRONYMS (continued)

Eu	Europium
EPMA	Electron probe microanalysis
FAS	Floridan aquifer system
Fe	Iron
Fe_2O_3	Ferric oxide
Fe_2O_3 (T)	Total iron
FeOOH	Iron oxyhydroxide
FeS_2	Pyrite or ferrous sulfide
FDEP/FGS	Florida Department of Environmental Protection/Florida Geological Survey
FIMS	Flow injection mercury system
FIU – FCEAM	Florida International University - Florida Center for Analytical Electron Microscopy
FUS-ICP	Fusion inductively coupled plasma
FUS-MS	Fusion mass spectrometry
FSU	Florida State University
g	grams
Ga	Gallium
Gd	Gadolinium
Ge	Germanium
HCO_3	Bicarbonate
HDO	High dissolved oxygen
Hf	Hafnium
HFO	Hydrous ferric oxides
Hg	Mercury
HNO_3	Nitric Acid
Ho	Holmium
H_2S	Hydrogen sulfide (gas)
I	Iodine
IC	Ion chromatography
ICP-MS	Inductively coupled plasma mass spectrometer
ICP-OES	Inductively coupled plasma optical emission spectrometer
INAA	Instrumental neutron activation analysis
In	Indium
Ir	Iridium
IR	Infrared
K	Potassium
kg	Kilogram
K2O	Potassium oxide
kV	Kilovolts
L	Liter

ABBREVIATIONS AND ACRONYMS (continued)

La	Lanthanum
LDO	Low dissolved oxygen
Li	Lithium
LOI	Loss on ignition
LLNL	Lawrence Livermore National Laboratory
Lu	Lutetium
MDL	Method detection limit
Mg	Magnesium
MgO	Magnesium oxide
µS	MicroSiemens
mg	milligram
mL	milliliters
Mn	Manganese
Mo	Molybdenum
mol	Mole
MnO	Manganese oxide
mV	millivolts
N_2	Nitrogen (gas)
Na	Sodium
Na_2O	Sodium oxide
nA	Nano angstroms
NOM	Natural organic material
Nb	Niobium
Nd	Neodymium
NGW	Native groundwater
Ni	Nickel
nm	Nanometer
NO_3	Nitrate
NSTS	North-South Transfer Station
O_2	Oxygen
ORP	Measured oxidation-reduction potential
Os	Osmium
Pb	Lead
Pd	Palladium
pH	negative log of the hydrogen ion concentration
ppb	parts per billion or µg/L
ppm	parts per million or mg/L
P_2O_5	Diphosphorus pentoxide
Pr	Praseodymium
Pt	Platinum

ABBREVIATIONS AND ACRONYMS (continued)

Q/K	Mineral saturation state
Rb	Rubidium
Re	Rhenium
REE	Rare earth elements
Ru	Rubidium
S	Sulfur
S_2	Sulfide
Sc	Scandium
Se	Selenium
Sec	Second
SEI	Secondary electron image
SEM	Scanning electron microscope
SO_2	Sulfur dioxide
SO_4	Sulfate
Sb	Antimony
SiO_2	Silica dioxide
Sm	Samarium
Sn	Tin
Sr	Strontium
SW	Source water
Ta	Tantalum
Tb	Terbium
TD-ICP	Total digestion, inductively coupled plasma
TDS	Total dissolved solids
Te	Tellurium
Th	Thorium
Ti	Titanium
TiO_2	Titanium dioxide
TITR	Titration
Tl	Thallium
Tm	Thulium
U	Uranium
UFA	Upper Floridan Aquifer
µg	microgram
µm	micron
V	Vanadium
W	Tungsten
WDS	Wavelength dispersive energy
XRF	X-ray fluorescence

ABBREVIATIONS AND ACRONYMS (continued)

Y	Yttrium
Yb	Ytterbium
Zn	Zinc
Zr	Zirconium

Geochemical Testing Program for the Cape Coral Aquifer Storage and Recovery System Pilot

Cindy Fischler, P.G. 2512, Paul Hansard, P.G. 2638 and Jonathan D. Arthur, P.G. 1149

INTRODUCTION

The purpose of this study is to evaluate water-rock hydrogeochemical processes at the bench scale for three Cape Coral Aquifer Storage and Recovery (ASR) wells. The core from one of the wells utilized techniques to ensure core preservation; the other two wells were left to atmospheric conditions. The scope of this study includes three main parts:
1) lithologic, geochemical and mineralogical characterization of aquifer rocks from the ASR storage zone as well as above and below the storage zone;
2) bench-scale leaching of selected ASR core samples to assess effects of variable dissolved oxygen (DO), redox conditions and core preservation techniques and
3) geochemical modeling of the bench-scale leaching (separate report).

Core used in this project was from three wells CPS-2 (W-18852), NSTS (W-18778) and CPS-4 (CPS-4). CPS-4 was the preserved core and attempts were made to prevent pyrite oxidation after the core was drilled. This is also the well used for all duplicate samples in the bench studies.

Simulated cycle tests employed in previous geochemical studies (e.g., Arthur et al., 2005) identified mobilization of trace metals and metalloids (hereafter referred to as "metals") from core material when exposed to high-DO (dissolved oxygen) conditions. Other researchers have identified the significance of DO with regard to metals mobilization during aquifer recharge (e.g., de Ruiter and Stuyfzand, 1998; Arthur et al., 2002; Pichler et al., 2004; Arthur et al., 2005). The bench-scale component of the present study is designed to evaluate three ASR operational approaches and identify water-rock reaction dynamics and processes associated with each approach under laboratory constraints utilizing preserved and unpreserved core. The three approaches (protocols) include:

- Experimental control (Low DO native groundwater and DO saturated source water)
- Degasification, removing DO utilizing Liqui-Cel™ contactors (source water only)
- Supersaturating with dissolved oxygen (source water only)

The bench-scale study is "reaction-kinetic" limited and is only an approximation of potential aquifer conditions during ASR activities, at least until ASR cycle-test data becomes available for comparison. Additional factors that constrain the application of bench-scale studies are ground-water mixing, effects of scale (i.e., study area size), water-rock ratios, physical and chemical aquifer heterogeneities (e.g., dual porosity), pressure-temperature differences, core preservation and microbial activity. While the bench-scale results may not have reached equilibrium conditions for all potential reactions, and are not expected to provide a direct comparison with water-quality changes observed during cycle testing at the Cape Coral ASR facility, prediction of relative degrees and perhaps magnitudes of metals mobilization may be realized. This information may prove to be a powerful predictive tool in the design, testing, and operation of ASR wells.

METHODS

Sample Preparation

Fifteen core samples were taken from each of the three wells (Figure 1) for a total of 45 samples (Table 1) for geochemistry and thin section analysis. Each well included a sample above the storage zone, below the storage zone and 13 samples from within the storage zone. Of the original 45 core samples from the three wells, only samples from within the storage zone were considered for the bench study.

Bench samples were chosen as follows: two samples from each of the wells with unpreserved core and three from the preserved core. The choice of which samples to use for the bench analysis was based on which of the thirteen storage zone samples had sufficient core material for all the analyses. Bulk (whole rock) geochemistry required up to 100 grams of powdered material. Thin section and microprobe analysis required one tab 1.1 x 1.8 inches (27 X 46 mm). Samples for bench-scale leaching of the unpreserved core required 900 grams of crushed core to make three 300 gram samples, one for each of the three bench protocol studies. The preserved core samples included an extra 300 gram split for sample duplicates (one for each protocol). Thus, a minimum of at least 1400 grams of crushed sample was targeted for each bench sample from the preserved core and 1100 grams for the unpreserved core. In terms of core length, each bench sample was comprised of approximately 6-12 inches (15.24 - 30.48 cm) of 4 inch (10.16 cm) diameter core.

Table 1. Lithogeochemical and thin section sample depths for all three wells. Underline indicates which samples were chosen for the bench study.

Core ID W-18778	Sample Depth Ft. BLS	Core ID W-18852	Sample Depth Ft. BLS	Core ID W-18849	Sample Depth Ft. BLS
NSTS	763.5-764	CPS-2	718.5-719	CPS-4	702-702.5
NSTS	839-839.5	CPS-2	833.5-834	CPS-4	817-817.5
NSTS	839.5-840	CPS-2	835-835.2	CPS-4	819.75-820
NSTS	840-841	CPS-2	836-836.5	CPS-4	830-830.75
NSTS	841-841.5	CPS-2	837.5-838.5	CPS-4	830.75-831
NSTS	843-843.5	CPS-2	838.5-839	CPS-4	831-831.25
NSTS	847.5-848	CPS-2	839.5-840	CPS-4	831.25-831.5
NSTS	848-848.5	CPS-2	840.5-841	CPS-4	831.75-832
NSTS	850-850.5	CPS-2	841.5-842	CPS-4	832-833
NSTS	851.5-852.5	CPS-2	842.5-843	CPS-4	833-833.5
NSTS	853-853.5	CPS-2	843-843.5	CPS-4	833.5-834
NSTS	854.5-855	CPS-2	843.5-844	CPS-4	834-835
NSTS	857-857.5	CPS-2	844-844.5	CPS-4	835-835.5
NSTS	858-859	CPS-2	844.5-845	CPS-4	835.5-836
NSTS	980.5-981	CPS-2	958-958.5	CPS-4	890-890.5

The preserved core CPS-4 (W-18849) was collected with attention to limiting its exposure to the atmosphere, thus minimizing effects of oxidation. After drilling, the core was wrapped in visqueen, and slid into a six-inch diameter PVC pipe with a PVC end cap glued on one end. Flex hose was inserted inside the PVC pipe down alongside the core as close to the bottom of the PVC pipe as possible. The PVC pipe was tilted up, the nitrogen tank was turned on, and nitrogen was allowed to evacuate the ambient air. When an adequate volume of nitrogen was injected in the bottom of the PVC pipe, the flex hose was quickly pulled out and the other PVC end cap was quickly glued on. It was then shipped to Florida Geological Survey (FGS) and remained in the PVC pipe unopened until sampling. As noted later in this report, the effectiveness of core preservation with respect to minimizing oxidation is not addressed.

Once sampled, all three wells had core section exteriors removed using a water-cooled trim saw. To minimize contamination, the trim saw is used solely for bench-scale leaching projects. Moreover, sample trimming was intended to remove drilling mud impregnated along the core exterior, post-drilling oxidized zones and precipitates (e.g., gypsum formed during core storage), as well as any possible anthropogenic contaminants. After trimming, each sample was rinsed with distilled de-ionized (DDI) water. The preserved core CPS-4 (W-18849) was placed in vacuum desiccators to dry and remained under vacuum until all samples were ready to crush and split. Core from the other two wells NSTS (W-18778) and CPS-2 (W-18852) were air-dried in a clean environment.

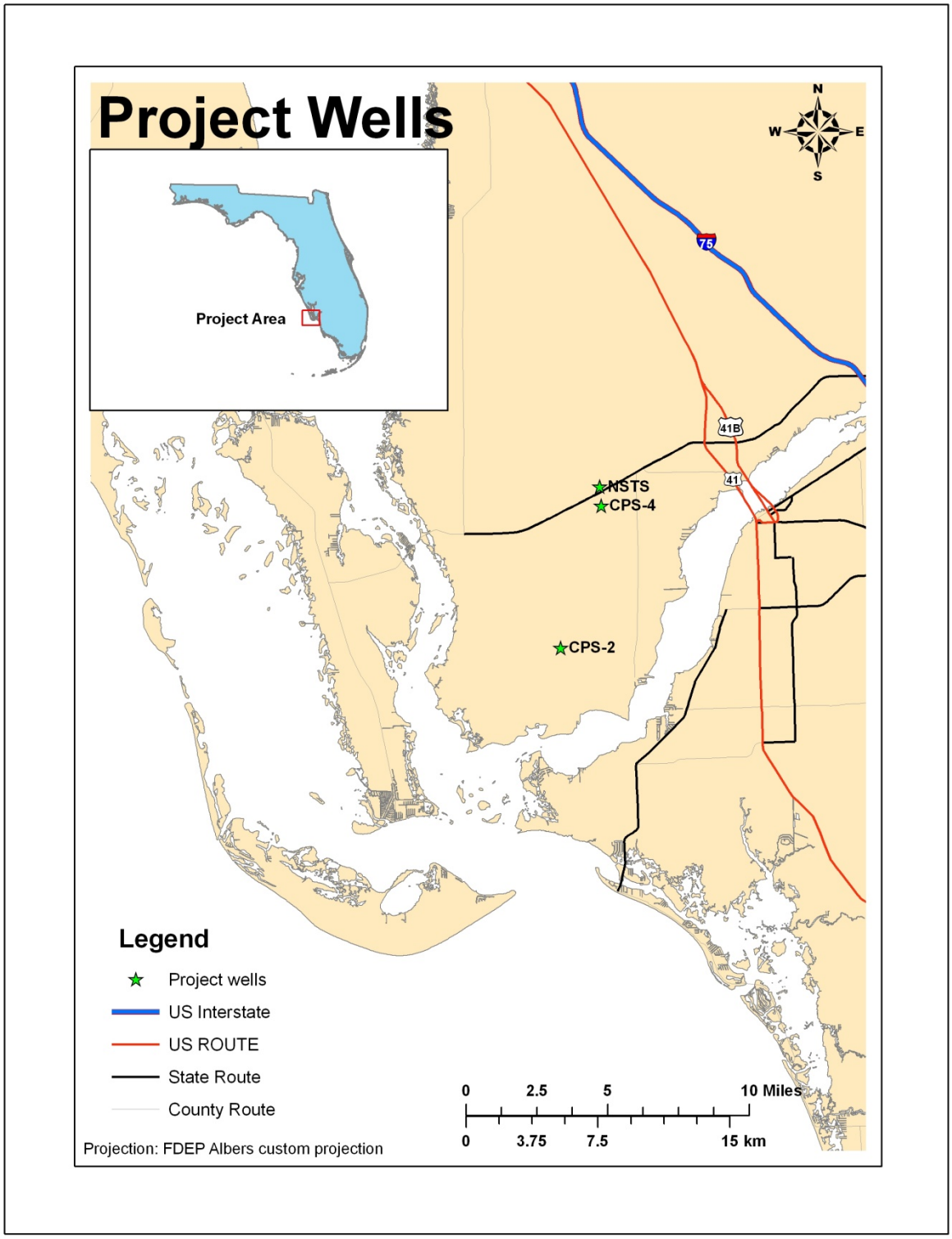

Figure 1. Location of wells sampled for this study.

Crushing, Splitting and Powdering

Dried core samples were crushed at the FGS using a Retsch BB100 jaw crusher set to 8-10 mm. The BB100 provided rapid gentle crushing of rock material using heavy metal free steel jaws. The rock crusher was cleaned with a nylon brush then vacuumed and jetted with compressed air. The removable sample compartment was washed and rinsed with DDI then 2-propanol and jetted with compressed air. After crushing, the rock chips were split using a Fritsch Rotary Cone Divider (Figure 2). The Fritsch unit was cleaned with a nylon brush, rinsed with DDI, then 2-propanol and jetted with compressed air. Rock powders were required for lithogeochemical analyses in this study. Pulverization was completed by Activation Laboratories Ltd. (Actlabs; analysis code RX4). Appendix 1 provides more detail on the pulverization procedure.

Figure 2. Fritsch rotary cone divider at FDEP/FGS Hydrogeochemistry Laboratory. This unit is accurate to within 0.42 percent, which is significantly better than the standard "cone and quarter" technique.

Scanning Electron Microscopy and Microprobe Analyses

Trace mineralogical analyses were completed using transmitted and reflected light microscopy, scanning electron microscopy (SEM), secondary electron backscatter imaging (BSE) and energy-dispersive x-ray (EDS) and wavelength dispersive spectrometer (WDS) electron probe microanalysis (EPMA). Polished thin sections were made at Spectrum Petrographics, Inc. Experimentation was completed to identify an impregnating/embedding resin for use in friable samples that did not contain measurable quantities of As and other trace metals. 3M Scotchcast #3 ™ was selected as an embedding material. Prior to image analyses, all thin sections were sputter-coated with carbon.

Microanalyses at the FDEP/FGS were completed using a JOEL JXA 840A electron probe microanalyzer. The unit consists of a main console which incorporates the electron optical column, secondary electron detector, Robinson backscatter electron detector (BSE), and EDS detector manufactured by X-ray Optics (Figure 3). 4pi Revolution software was utilized for microanalysis and imaging, including energy spectra. Energy-dispersive analyses had a 100-second acquire time, with a dead time between 25-35. The working distance was 39 mm and the stage was set to zero tilt. Electron probe current ranged from 9 to 10 nannoamps (nA) and the SEM operating voltage was 20 kV. Secondary electron (topographic) imagery is useful to identify textures, while BSE images enhance contrast between different minerals or mineral compositions based on the average atomic number; the brighter the mineral the higher its average atomic number.

Figure 3. FDEP/FGS microanalysis laboratory (left) and the electron probe microanalysis laboratory at the FIU-FCEAM facility (right).

Quantitative electron probe microanalyses (EPMA) were completed on-site (and remotely via the Internet) at the Florida Center for Analytical Electron Microscopy (FCAEM) at Florida International University (http://www.fiu.edu/~emlab/inst_EPMA.html) using a JEOL 8900R Superprobe with five 2-crystal detectors (Figure 3). Quantitative analyses of minerals in polished, carbon-coated thin sections were completed using a 20 nA probe current. Each analysis included 8 elements (see Table 2 for element conditions). According to the lab, analytical detection limits for all metal analyses and element maps was approximately 100 parts per million (ppm).

Geochemical Procedures

This section not only describes the analytical methods for rock and water chemical analyses, but also methods designed and employed for bench-scale analyses of aquifer matrix samples. Electron microprobe analytical procedures are described in the prior section. Addressing significant figures in this report was a challenge due to limitations of data-management software and inconsistencies in laboratory reporting. For consistency herein, the number of decimal places in analytical detection limits (DL) was applied. Tables and appendices in this report denote concentrations less than the DL for a particular analyte as "<" for hydrogeochemical results or BDL for lithogeochemical results. The DL may vary for hydrogeochemical analyses due to sample dilution because of matrix interference.

Table 2. Electron probe microanalyses (EPMA) element conditions for geochemical standard and unknown analyses.

	Elem- 1	Elem- 2	Elem- 3	Elem- 4	Elem- 5	Elem- 6	Elem- 7	Elem- 8
Elements	Mg	Fe	S	As	Ca	Mo	U	Sb
Name	Mg	Fe	S	As	Ca	Mo	U	Sb
X-ray Name	Ka	Ka	Ka	Ka	Ka	La	Ma	La
Order	1	1	1	1	1	1	1	1
Channel	1	2	3	2	3	2	3	2
Crystal	TAP	LIF	PETJ	LIF	PETJ	PETJ	PETJ	PETJ
Spect. Pos.(mm)	107.467	134.650	172.101	81.569	107.567	173.228	125.168	110.083
Back (+) (mm)	11.500	5.000	5.500	7.000	8.500	6.000	5.000	6.000
Back (-) (mm)	11.000	5.000	5.500	5.000	9.000	8.000	5.000	5.000
Time/Count	Time	Time	Time	Time	Time	Time	Time	Time
Peak Seek W.	1	1	1	1	1	1	1	1
Mes. Time (sec)	10.0	20.0	20.0	150.0	10.0	100.0	100.0	100.0
Bac. Time (sec)	5.0	10.0	10.0	60.0	5.0	30.0	30.0	30.0
Mes. Count	10000	10000	10000	10000	10000	10000	10000	10000
Bac. Count	500	500	500	500	500	500	500	500
PHA gain	32	32	128	32	64	128	64	64
High V.(V)	1698	1730	1672	1666	1690	1674	1720	1700
Base L.(V)	2.00	0.40	0.50	0.50	1.00	0.50	0.50	0.50
Window (V)	5.00	9.40	8.00	9.00	6.00	8.50	9.00	8.00
Diff/Int	Diff	Diff	Diff	Diff	Diff	Diff	Diff	Diff
Sequence	1	1	1	2	2	3	3	4

Lithogeochemistry

Major, trace, and rare earth element geochemical analyses were completed at a commercial laboratory (Activation Laboratories, Ltd. [Actlabs], Ancaster, Ontario, Canada) for 45 rock samples (Appendix 2). The multi-method analytical package (4E-Research) included use of these analytical methods: 1) inductively coupled plasma - optical emission spectrometer (ICP-OES), 2) trace element fusion inductively coupled plasma - mass spectrometer (ICP/MS), 3) instrumental neutron activation analysis (INAA), and 4) x-ray fluorescence spectrometer (XRF). Carbon and Sulfur were analyzed using an automated LECO CS-344 analyzer and a solid-state infra-red detector to yield CO_2, total C, graphitic C, organic C, S and SO_4. A Perkin Elmer Flow Injection Mercury System (FIMS) 100 cold vapor Hg analyzer was used for all samples.

Actlabs utilizes a lithium metaborate/tetraborate fusion process, followed by acid digestion to ensure total metal recovery, particularly for rare-earth elements (REEs) in resistate phases. This method is employed because standard acid digestions of refractory minerals (e.g., zircon, sphene, etc.) may be incomplete. The trace element package by ICP/MS on the fusion solution provides research quality data whether using standard or research detection limits. The "Code 4E Research" analytical package combines ICP, INAA, ICP/MS and XRF technologies to completely characterize geological samples using the optimum method for individual constituents. The package provides lower (research-grade) detection limits that are among the best of those commercially available. These detection limits are suitable for geochemical modeling needs. More detailed description of these analytical procedures are included in Appendix 1. A previous CERP study (Arthur et al., 2007b) included 50 samples which were analyzed in duplicate for precision analysis and analyses of geochemical standards as unknowns (observed versus expected) were also completed to assess analytical accuracy of the lab. Results are found in that report.

Hydrogeochemistry

Water-sample compositions from bench-scale leaching studies were determined at Actlabs using ICP/MS and ICP/OES (if "over-range" was required). Cation analyses for water samples (e.g., source and groundwater analyses and leachability samples) were completed using Actlabs "Code 6 – ICP/MS". Anions for water (leachate) samples were analyzed by ion chromatography "Code 6B" using EPA reference method 300.0. For method descriptions see Appendix 1.

Bench-Scale Leaching

Bench-scale leaching followed three separate protocols that varied according to contract requirements and the results of prior bench studies, including those of Arthur and Dabous (2007), Arthur et al. (2007a, 2007b, 2007c) and Arthur et al. (2008). The samples were set up as three separate bench-scale studies (Table 3). Protocol 1 used native groundwater and source water as the leachates, while Protocols 2 and 3 used only source water. Native groundwater was collected from each of the three well sites (CPS-2, CPS-4, and NSTS) and the source water was collected from the Canal Pump Stations (CPS-2 and CPS-4 well site). This was the source water expected to be used for future ASR activities.

Water Collection

Ten liter carboys were filled by Ed Rectenwald of MWH Americas. Water was immediately shipped to the FDEP/FGS Hydrogeochemistry Laboratory and refrigerated. There was an effort to minimize UV/sunlight exposure after collection. The native groundwater was collected from each ASR site (CPS-4, CPS-2 and NSTS) intended to be used with the corresponding core samples from each well. Compressed nitrogen gas was streamed into the headspace while filling the carboys with native groundwater in an effort to maintain DO and ORP (oxidation-reduction potential) values. Source water was only available from two sites Canal Pump Station 2 and 4 (CPS-2, CPS-4). Source waters from the canal pump stations were collected after going through the filtration and chlorination processes. The NSTS site did not have a pump station so CPS-4 water was used for core samples from that well.

Bench-Scale Analysis Protocols

The protocols/procedures employed in this study were intended to address specific hypotheses related to ASR water-rock chemical reactions. This work was designed to evaluate water-rock hydrogeochemical processes at the bench scale in order to characterize what may be encountered in the field during cycle testing.

The ratio of core chips to leachate used in the bench-scale leaching experiments was derived from previously measured As in ASR cycle-test field data (using 20 µg/L As) and a "high average" As concentration in the aquifer matrix (5 ppm). This combination yields 0.4 percent leaching of total As in the rock. With this amount of leaching, 300 g of rock with 5 ppm As would yield concentrations in the leachate above the As detection limit and within the range of observed As in ASR recovered water.

Table 3. Reaction Vessel numbers in bench-scale leaching study; Blank = geochemical control.

Core ID	Sample Depth Ft. BLS	Source water locale	Protocol 1 Vessel #	Protocol 2 Vessel #	Protocol 3 Vessel #
NSTS (W-18778)	840-841	CPS-4	1	1	1
NSTS (W-18778)	851.5-852.5	CPS-4	2	2	2
CPS-2 (W18852)	837.5-838.5	CPS-2	3	3	3
CPS-2 (W18852)	842.5-843	CPS-2	4	4	4
CPS-4 (W18849)	830-830.75	CPS-4	5	5, 6 duplicate	5
CPS-4 (W18849)	832-833	CPS-4	6	7	6, 7 duplicate
CPS-4 (W18849)	834-835	CPS-4	8, 9 duplicate	8	8
Blank	N/A	CPS-4	7	9	9

The bench-scale studies consisted of three separate protocols (Tables 4-6). The three protocols were designed to 1) explore different treatment methods of source water under consideration for the three ASR sites as well as 2) investigate the effect of core preservation on bench-scale studies. Each protocol consisted of a blank (water only), three samples from CPS-4 "preserved core"; two samples from CPS-2 and two samples from NSTS (Table 3). Core from CPS-2 and NSTS were not preserved. There was also one duplicate for each protocol which used

the preserved core CPS-4. All protocols started with a new split of 300 grams of crushed core sample (maximum chip size was 10 mm) added to the reaction vessels (Figure 4). One liter of the appropriate water was slowly added, taking care not to scatter the rock sample. After all reaction vessels were filled, a vacuum was applied to pull fluid into the rock pore space and remove air bubbles. After applying the vacuum the 1L level was marked on the vessel. The following day specific conductivity, DO, ORP (relative to the Ag/AgCl electrode), pH and temperature were measured for each vessel. Water samples were then collected: 18 mL for ICP-MS and ICP-OES (for over-range analyses if needed), and 2 mL for anions. The 18 mL sample was centrifuged at ~3,800 rpm for five minutes then decanted and preserved with 0.2 mL HNO_3 (diluted 1:1). No preservative was needed for the 2 mL anion sample; however, during collection, the anion samples were syringe-filtered (Figure 4).

When a leachate change was required in preparation for the next experimental phase (Tables 4-6) water was siphoned out of each reaction vessel into a Millipore filter (Millipore Omnipore membrane 1.0 µm) funnel. The water was pulled through the filter by low vacuum and as much water as possible was removed from the reaction vessels. Prior to adding the water for the next phase, suspended material caught on the filter was washed into the vessel using the new water. If multiple filters were needed due to clogging, all filters were washed into the reaction vessel. A sample was collected from the new water to be used as a geochemical leachate reference. The appropriate "new" water was added using a peristaltic pump and each vessel was gently filled to the 1L mark.

Per the schedule outlined for the three protocols (Tables 4-6), all vessels were sampled for cation and anion analyses (2.0 mL for anions and 18 mL for cations) and measured for the above mentioned physical parameters. After measuring physical parameters and sampling, the volume of water removed for analysis was replaced by adding 20 mL of the appropriate water to the vessels. The last sampling event before a water change included a sample for alkalinity.

Protocol 1 was initiated (Phase 1) using native groundwaters that had been sparged with 95/5 percent N_2/H_2S gas to induce low-DO (LDO), low-ORP conditions. A N_2 headspace was maintained throughout this phase. The purpose was to establish equilibrium between water and rock. Native groundwater (NGW) was used to simulate native conditions in the aquifer (low dissolved oxygen < 0.3 mg/L and low ORP <-200mV). Under these conditions pyrite should be stable in the presence of NGW. Sampling and parameter measurements were completed as previously described and listed in Table 4. The vessels were re-sparged with H_2S if ORP measurements approached -200mV or higher. Phase 2 followed a water change to the appropriate source waters as described above. The source water was a high-DO (HDO) condition, with similar frequency of sampling. A room air headspace was maintained. The purpose was to simulate recharge of source water into an aquifer which is under reduced conditions and assess oxidation of arsenic phases under traditional ASR conditions.

Protocol 2 was initiated (Phase 1) using the source water sparged with 95/5 percent N_2/H_2S (gas) to address reductive dissolution (negative ORP) of FeOH formed by exposure of the core to the atmosphere. Sampling and parameters were completed as described above and in Table 5. A N_2 headspace was maintained for all phases. Phase 2 followed a water change using the source water sparged with 95/5 percent N_2/H_2S (gas) to further address reductive dissolution (negative ORP) of Hydrous ferric oxides (HFO) formed by exposure of the core to the atmosphere, in an attempt to remove the FeOOH formed by oxidation of pyrite. Sampling was as above and in Table 5. Phase 3 followed a water change using source waters which had gone through Liqui-Cel™ contactors to strip most of the O_2 out of the water (Figure 5). The purpose was to see if the small amount of DO would be enough to oxidize the pyrite. The DO after Liqui-

Cel™ treatment was between 300-500 µg/L to approximate the DO levels of water after processing through a stripping tower; one of the plans under consideration for the ASR site was to use a stripping tower to lower DO before recharge. Liqui-Cel™ water ORP values (relative to an Ag/AgCl electrode) were between 230 to 250 mV before adding to the reaction vessels. After adding to reaction vessels the ORP and DO dropped significantly, probably due to residual water sparged with H_2S from Phase 2.

Protocol 3 utilized source waters sparged with a 1:1 mix of O_2/N_2 gas to address the effects of water supersaturated in DO in relation to arsenic from the oxidation of pyrite. An O_2/N_2 (1:1) headspace was maintained for phases 1-3. Sampling and parameters were completed as described above and in Table 6. Phases 2 and 3 involved water changes but the conditions were identical to Phase 1. During Phase 1 through 3 the DO was maintained between 18 to 21 mg/L. Phase 4 water change involved source water "as is" (DO saturated ~8.5mg/L with no treatment or sparging), to assess oxidation of arsenic phases after repeated exposure to supersaturated DO. A room air headspace was maintained during this last phase. Results of all three protocols are discussed in a later section of this report.

Figure 4. Sealed reaction vessels with N_2 (gas) lines (left) and filtered sampling for anions analyses (right).

Figure 5. Liqui-Cel™ membrane contactors lab set-up (left) close up of contactors (right).

Table 4. Protocol 1 for the bench-scale leaching study.

Project phase	**1**	**2**	
Cumulative timeline (number of weeks at end of phase)	2	8	
Phase duration	2 weeks	6 weeks	
Type of leachate	Native groundwater (sparged with H2S)	Source Water	
Reaction vessel head space	N2 (gas) (2,3)	Air (1)	
Processes to address	Establish equilibruim between water and rock	Stabilize DO, ORP, obtain background analyses; assess oxidation of As phases	
Sampling frequency for hydrogeochemistry	3X/week first week, then 2X/week	3x/week first week then 2X/week	
Sampling frequency for physical parameters	3X/week first week, then 2X/week	3x/week first week then 2X/week	
Phase-specific comments		Replace native groundwater with source water	
Overall comments:	Each sampling event is replaced with an equal volume of original leachate water (NGW or SW)		
	Analyses will include standard multi-metal, multi-method hydrogeochemistry package plus anions, DO, T, ORP, pH, EC		
	Geochemical blank and duplicate with core-chip split will be sampled and analyzed		
	Modified hungate technique will be employed during sampling of low-DO leachate		
	Spinning riffling splitter (Gilson Co., Inc.) was used to obtain duplicate set of core chips; accurate to within 0.42%		
	Leachate samples for cation analyses are cetrifuged; anion samples are microfiltered (0.45 um)		
Footnotes (x):	(1) Sparge with air recognizing that CO2 in air reduces pH, which although buffered at field scale, is not efficiently buffered at bench scale.		
	(2) Pull vacuum on all vessels to maximize infiltration of leachate water into rock matrix		
	(3) Induce N2 (gas) head space to reduce/maintain low DO.		

Table 5. Protocol 2 for the bench-scale leaching study.

Project phase	1	2	3
Cumulative timeline (number of weeks at end of phase)	2.5	8	12
Phase duration	2.5 week	5.5 week	4 week
Type of leachate	Source water (SW) Sparge with H2S LDO and -ORP	Source Water (new SW) Sparge with H2S LDO and -ORP	Source Water (new SW) LDO using Liqui-cel (DO ~300-500 ppb)
Reaction vessel head space	N2 (gas) (1,2)	N2 (gas) (2)	N2 (gas) (2)
Processes to address	Reductive dissolution (-ORP) of FeOH formed by exposure of core to atmosphere	Reductive dissolution (-ORP) of FeOH formed by exposure of core to atmosphere	Stabilize, establish equilibrium between water and rock. DO high enough to oxidize pyrite??
Sampling frequency for hydrogeochemistry	3X/week	2X/week	First week 4X/week then 3X/week for 3weeks then 2X/week for 2 weeks
Sampling frequency for physical parameters	3X/week	2X/week	First week 4X/week then 3X/week for 3weeks then 2X/week for 2 weeks
Phase-specific comments		Replace old source water with H2S source water	Replace old source water with source water using liqui-cel to get DO below 5ppb (No H2S)
Overall comments:	Each sampling event is replaced with an equal volume of original leachate water (SW)		
	Analyses will include standard multi-metal, multi-method hydrogeochemistry package plus anions, DO, T, ORP, pH, EC		
	Geochemical blank and duplicate with core-chip split will be sampled and analyzed		
	Modified hungate technique will be employed during sampling of low-DO leachate		
	Spinning riffling splitter (Gilson Co., Inc.) was used to obtain duplicate set of core chips; accurate to within 0.42%		
	Leachate samples for cation analyses are cetrifuged; anion samples are microfiltered (0.45 um)		
	Phase 3 --Source water put through liqui-cell contactors at room temp. no additional steps taken to lower ORP		
Footnotes (x):	(1) Pull vacuum on all vessels to maximize infiltration leachate water into rock matrix		
	(2) Induce N2 (gas) head space to reduce/maintain low DO.		

Table 6. Protocol 3 for the bench-scale leaching study.

Project phase	1	2	3	4
Cumulative timeline (number of weeks at end of phase)	3	6	9	12
Phase duration	3 weeks	3 weeks	3 weeks	3 weeks
Type of leachate	Source water (SW) DO ~19-20mg/L	Source water (new SW) DO ~19-20mg/L	Source water (new SW) DO ~19-20mg/L	Source Water (new SW)DO ~8mg/L
Reaction vessel head space	Supersaturate with 50/50 O2/N2 mix	Supersaturate with 50/50 O2/N2 mix	Supersaturate with 50/50 O2/N2 mix	Room Air
Processes to address	Evaluate rock-water interaction under supersaturated DO conditions	Evaluate rock-water interaction under supersaturated DO conditions	Evaluate rock-water interaction under supersaturated DO conditions	Evaluate rock-water interaction under saturated DO conditions
Sampling frequency for hydrogeochemistry	everyday 1st wk then 2X/week	everyday 1st wk then 2X/week	everyday 1st wk then 2X/week	everyday 1st wk then 2X/week
Sampling frequency for physical parameters	everyday 1st wk then 2X/week	everyday 1st wk then 2X/week	everyday 1st wk then 2X/week	everyday 1st wk then 2X/week
Phase-specific comments		Replace old source water with supersaturated source water	Replace old source water with supersaturated source water	Replace old source water with source water at saturated DO (~8mg/L)
Overall comments:	Each sampling event is replaced with an equal volume of original leachate water (SW)			
	Analyses include standard multi-metal, multi-method hydrogeochemistry package plus anions, DO, T, ORP, pH, EC			
	Geochemical blank and duplicate with core-chip split is sampled and analyzed			
	Spinning riffling splitter (Gilson Co., Inc.) is used to obtain duplicate sets of core chips; accurate to within 0.42%			
	Leachate samples for cation analyses are cetrifuged; anion samples are microfiltered (0.45 um)			

RESULTS

Lithologic and Hydrogeological Properties

All samples for the bench study are from the ASR storage zones. The storage zones for each well are as follows: CPS-4 780-870 feet (ft) below land surface (BLS), CPS-2 780-860 ft BLS and NSTS 800-920 ft BLS. All bench samples are collected from within the Suwannee Limestone with three samples from preserved core CPS-4 and four samples (2 from each well) unpreserved core NSTS and CPS-2. In the study area, this lithostratigraphic unit is predominately a biomicrite with a medium grained texture. It consists of foraminifera, peloids, echinoids, mollusk fragments and some coral. Finely disseminated natural organic matter (NOM) is observed throughout and locally as wispy laminae. Grain sizes are generally microcrystalline to medium and induration is moderate to good. Cements include dolomite, calcilutite and sparry calcite. A detailed description of the samples (lithogeochemical and bench leaching) is provided in Appendix 3.

Hydrogeological data from the ASR storage zone for NSTS and CPS-4 are reported from MWH and City of Cape Coral completion reports (2009, 2010) as follows. Hydraulic conductivity measurements were made in accordance of ASTM Standard D 5084 "Measurement of hydraulic conductivity of saturated porous materials using a flexible wall permeameter" using constant head. For core CPS-4, values for vertical hydraulic conductivity analyses at 818.2 and 835.6 ft BLS respectively are $1.0E^{-07}$ cm/sec and $6.8E^{-04}$ cm/sec ($2.8E^{-04}$ ft/day and 1.9 ft/day) and the horizontal hydraulic conductivity values are $4.1E^{-07}$ cm/sec and $1.6E^{-03}$ cm/sec ($1.16E^{-03}$ ft/day and 4.5 ft/day). For core NSTS, values for vertical hydraulic conductivity analyses at 842.5 and 846.8 ft BLS respectively are $8.3E^{-07}$ cm/sec and $2.4E^{-04}$ cm/sec ($2.35E^{-03}$ ft/day and 0.68 ft/day) and the horizontal hydraulic conductivity at 846.8 ft BLS (only one value given) is $4.6E^{-04}$ cm/sec (1.30 ft/day). Vertical porosity values for the storage zone of CPS-4 at 818.2 and 835.6 ft BLS respectively are 41.6 percent and 44.4 percent; values for NSTS at 842.5 and 846.8 ft BLS are 30.6 percent and 41.1 percent. Horizontal porosity values for the storage zone of CPS-4 at 818.2 and 835.6ft BLS are 43.9 percent and 43.0 percent; the value for NSTS at 846.8ft BLS (only one value given) is 40.4 percent. Hydrogeological data was not available for CPS-2.

Mineralogy and Mineral Chemistry

Mineralogy of samples for which lithogeochemistry was completed is relatively simple. The limestones are comprised of calcite with quartz sand grains and trace amounts of dolomite, clay, carbonate fluorapatite, pyrite, glauconite and NOM. CPS-2 also had small amounts of gypsum and halite forming on some of the thin sections, possibly a precipitate from the original native groundwater while drying. Trace amounts of carbonate fluorapatite was observed in several of the thin sections. Quartz sand was observed in thin sections from trace amounts to 3-5 percent.

All 45 thin sections were looked at microscopically with transmitted and reflected light; a compilation of those photomicrographs are found in Appendix 4. Thin section preparation included vacuum embedding with a blue-dye epoxy so that open pore space would show blue in the thin sections. All thin section preparation was done by Spectrum Petrographics Inc.

Figure 6 is a pyrite framboid in reflected and transmitted light. In transmitted light, the pyrites as well as other heavy minerals and air filled spaces are opaque and not easily distinguished from each other; add reflected light and the pyrites and other heavy minerals become readily apparent (Figure 7). In reflected light it can be difficult to distinguish euhedral grains of pyrite from other heavy minerals but larger framboids are easily identified (Figures 6-8). It appears in reflected light some of the pyrites show signs of oxidation, further microprobe investigation of these specific areas may provide insight into this hypothesis (Figure 9). Also observed were rounded green mineral grains that are possibly glauconite (Figures 10 and 11).

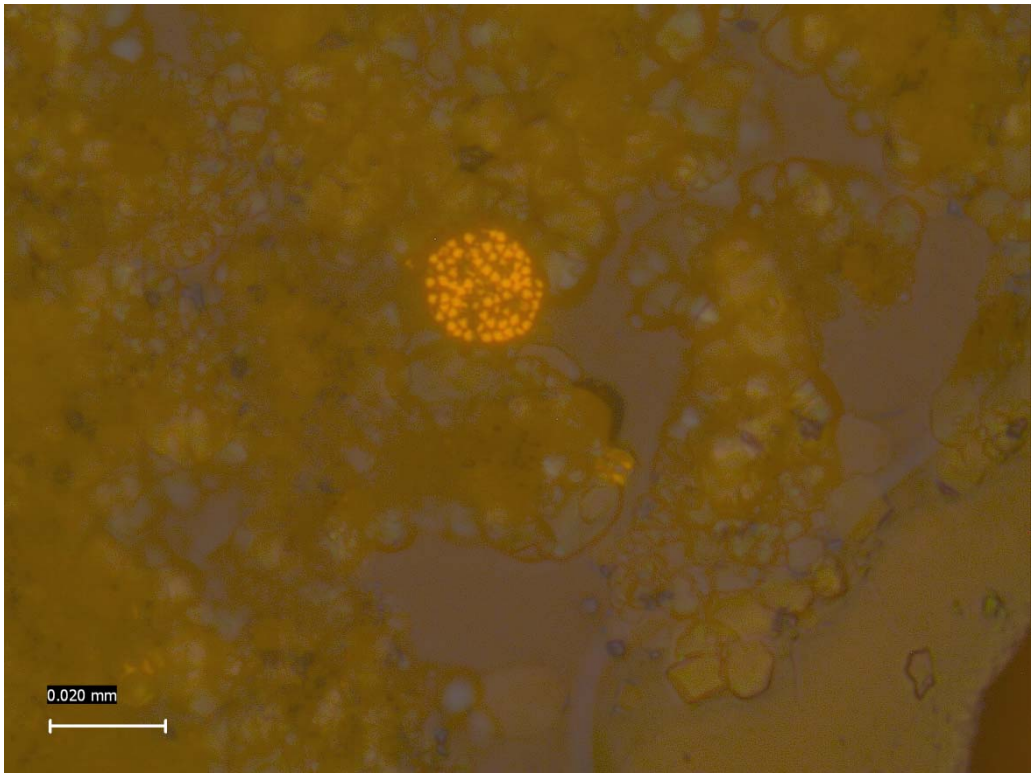

Figure 6. Pyrite framboid with transmitted and reflected light CPS-4 831.75-832 ft BLS.

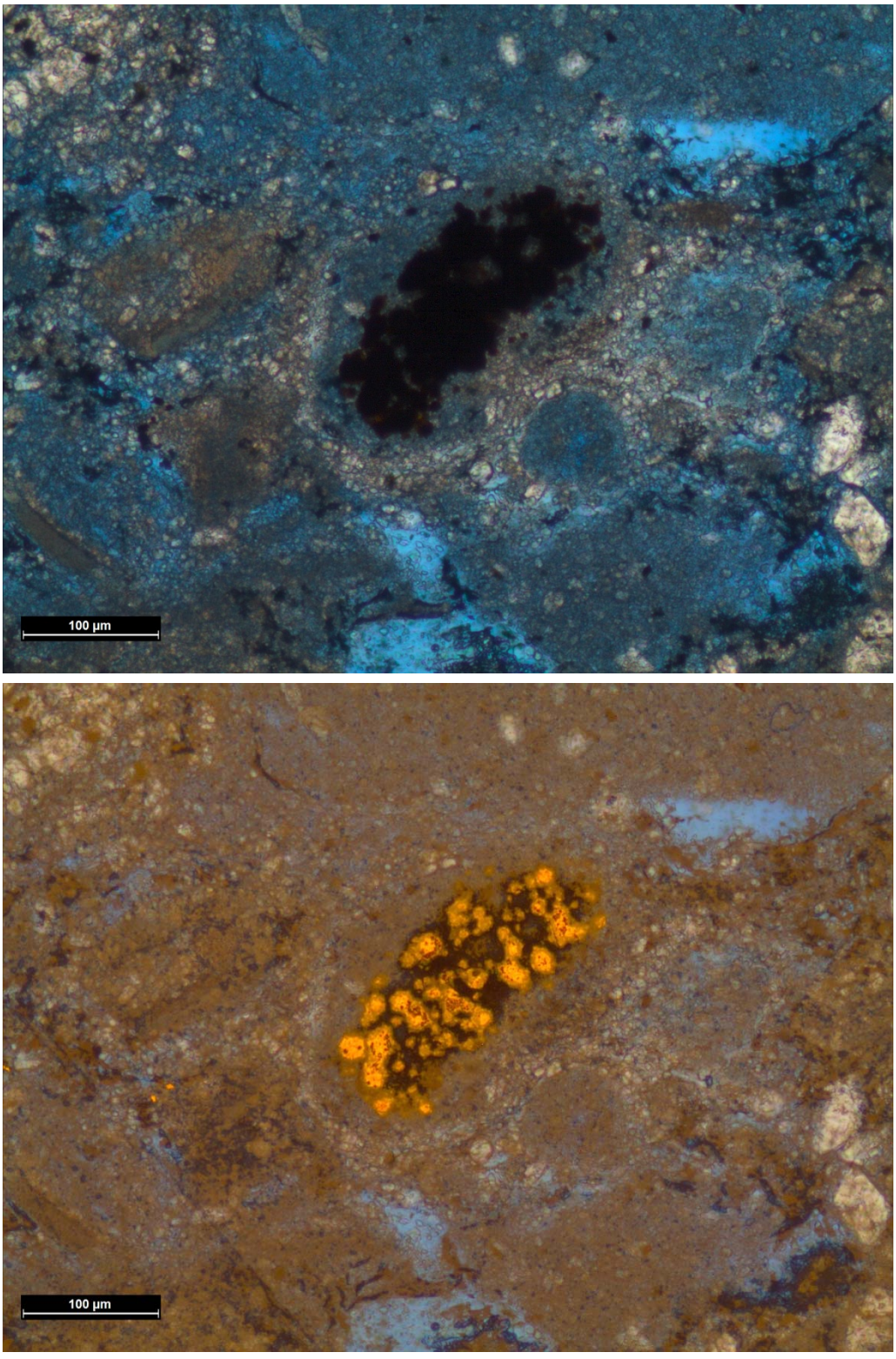

Figure 7. Pyrite framboid cluster in transmitted light (upper), and same image in reflected and transmitted light (lower) CPS-2 835-835.2 ft BLS.

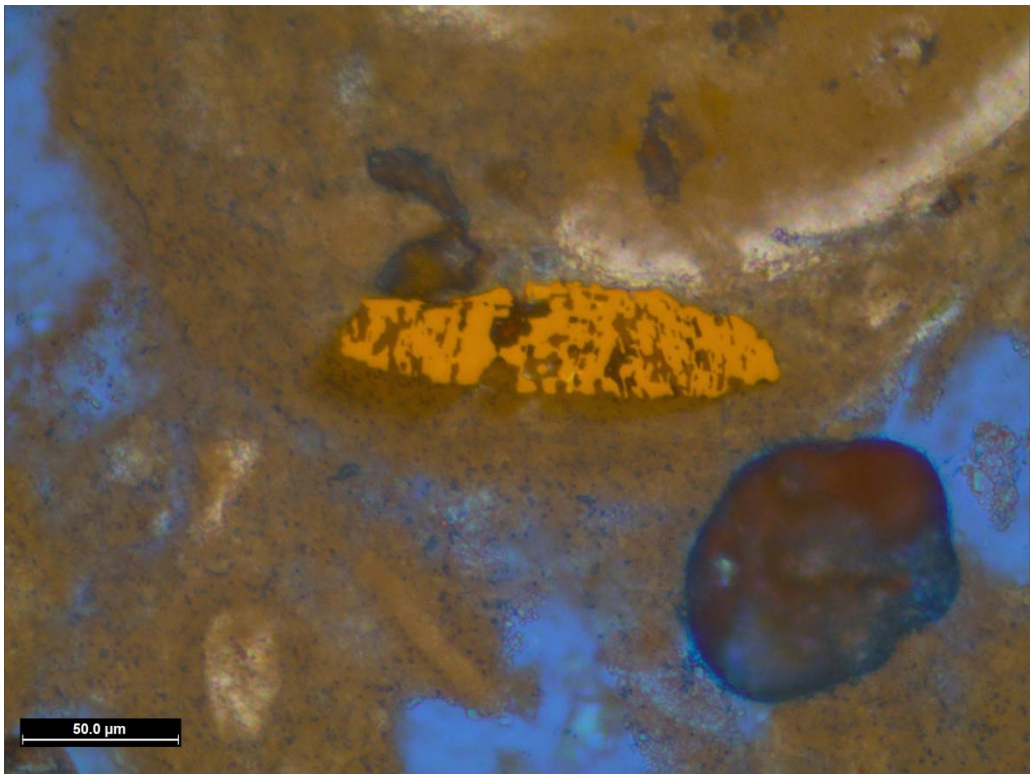

Figure 8. Heavy mineral possibly ilmenite with transmitted and reflected light CPS-2 841.5-842 ft BLS.

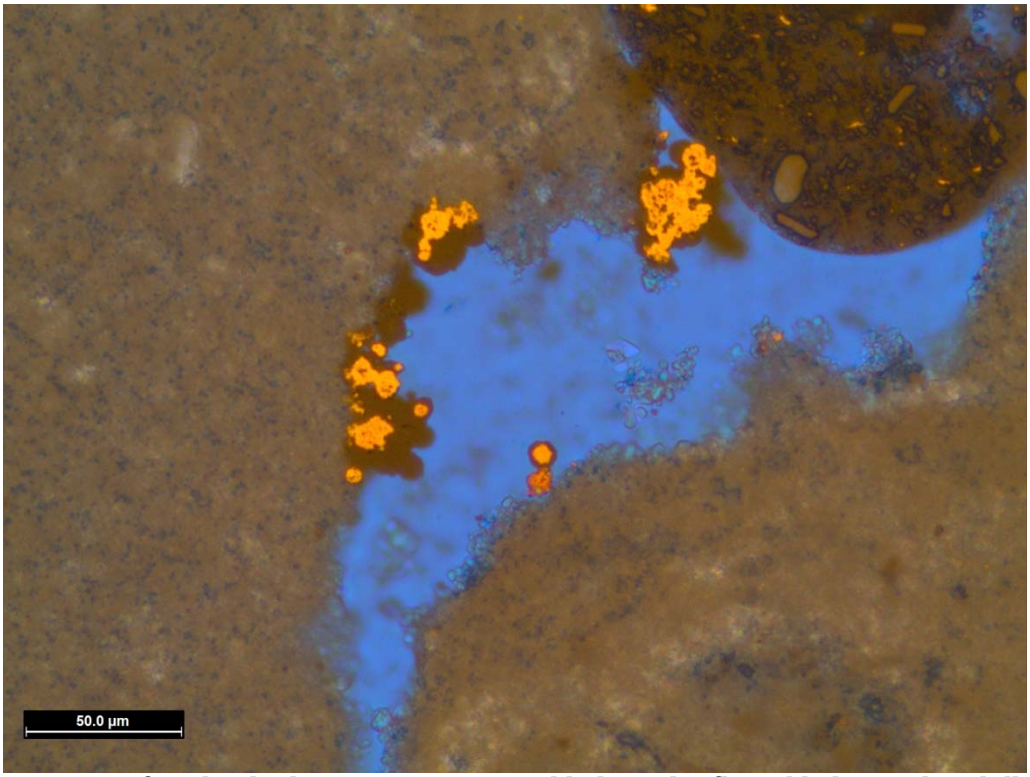

Figure 9. Pyrite framboids clusters in transmitted light and reflected light. Darker dull areas around the brighter pyrites may be evidence of pyrite oxidation CPS-2 839.5-840 ft BLS.

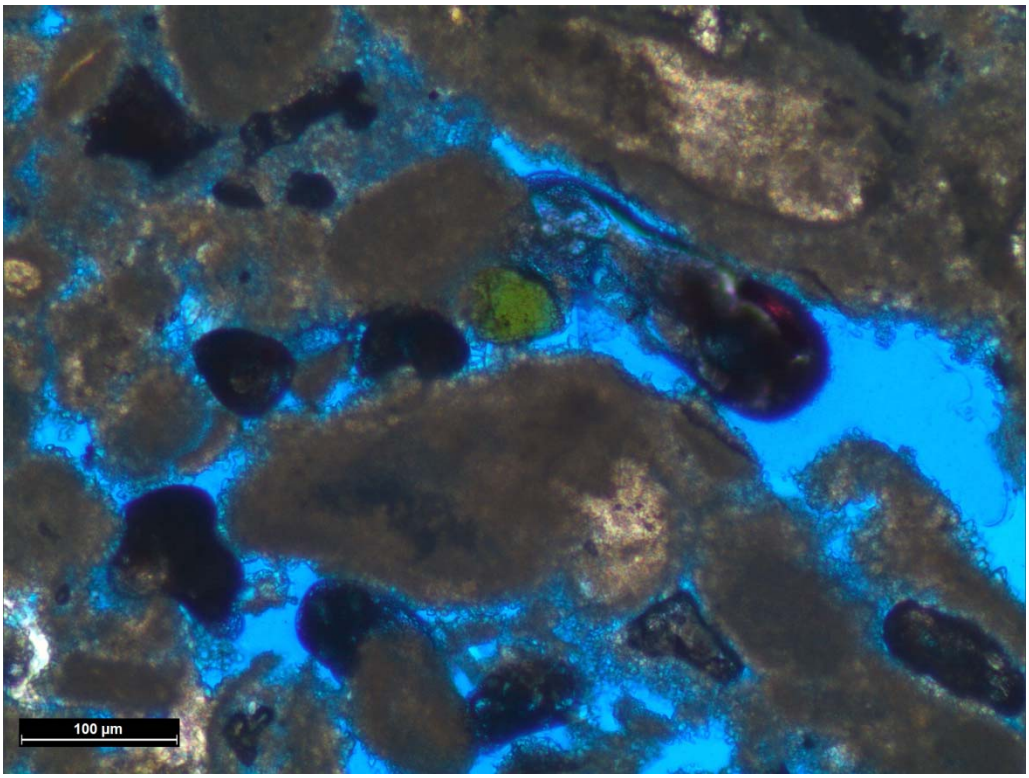

Figure 10. Possible glauconite in transmitted light. CPS-2 844.5-845 ft BLS.

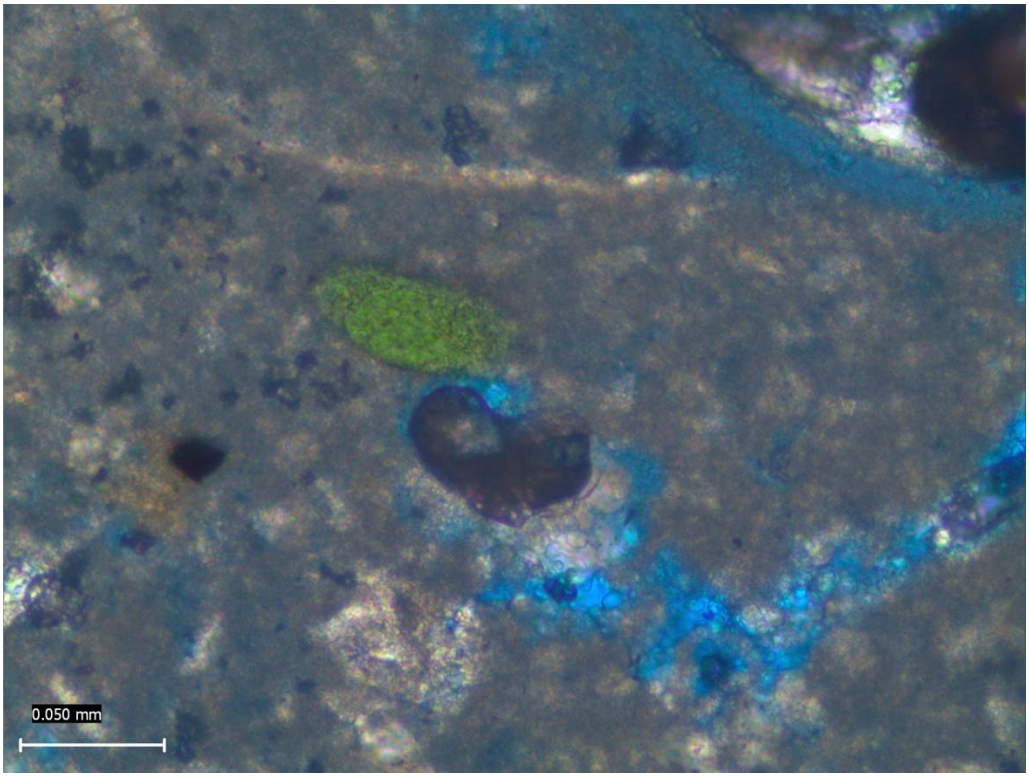

Figure 11. Possible glauconite in transmitted light CPS-4 835-835.5 ft BLS.

Polished thin sections were examined by SEM-EDS and EPMA to identify trace minerals and determine qualitative or quantitative trace-metal compositions. Pyrites occur as framboids, euhedral crystals and anhedral clusters possibly due to replacement (Figures 12 -14). Pyrites were found in all 45 thin sections by transmitted and reflected light and or SEM-EDS and EPMA. Figure 12 is a secondary electron image (SEI) of a typical pyrite framboid. Figure 13 is a SEI of an unaltered, euhedral pyrite crystal. Figure 14 is a SEI of pyrite framboids and anhedral clusters of pyrite. Appendix 5 provides a compilation of additional SEM images and element maps and spectra (both EDS and wavelength dispersive [WDS] X-ray microprobe).

Quantitative EPMA utilizing WDS was completed for pyrites observed in several thin sections from each of the three wells. Thin sections chosen for EPMA analysis were all of the bench study thin sections and other sections which included detects for As in the lithogeochemical analyses. From these thin sections approximately 250 analyses were completed, about 155 on pyrites and the remainder on carbonates and other minerals. Analysis of carbonates included carbonate mud, matrix, spar, calcite crystals and shell material. EDS analyses were completed for any thin sections not analyzed by EPMA. EDS focused on minerals of high-average atomic number with an emphasis on pyrite abundance and morphology. EDS does not discern elemental compositions less than approximately two weight percent, while EPMA detection limits are approximately 100 ppm (0.01 percent) per personal communication from Tom Beasley (FIU FCAEM). Appendices 6-8 lists selected WDS analytical results anything below the analytical detection limit is listed as below detection limit (BDL).

Reconnaissance EDS analyses detected several minerals including ilmenite, rutile, gypsum, zircon, quartz and pentlandite. The following elements were analyzed by EPMA: Mg, Fe, Ca, As, S, Mo, Sb and U (Table 2). Total weight percent in Appendices 6-8 may not be 100 percent as other elements may be present for which we did not analyze, analyses were set up for metals and not oxides, hence, oxygen would not be included in the totals. Some pyrites may have measureable amounts of calcite due to the beam size in relation to the pyrite size. The pyrite may be so small that the beam will include a small part of the matrix in the analysis. Figure 15 is an element map of an arsenopyrite crystal from CPS-4 835-835.5 ft BLS. The element map for Fe, S and As has distinct patterns reflecting arsenopyrite while the Ca reflects the surrounding calcite. Also note the faint pattern of U and V (this element map included V and not Sb) in association with the pyrite. Figure 16 is an EDS spectrum of the arsenopyrite in Figure 15. Trace metal associations with pyrites, based on EPMA analyses of the three wells in appendix 6-8, include As, Mo and U while Sb appeared to be more closely associated with the carbonate fraction (Appendices 6-8). Arsenic has also been observed in the EPMA data for the carbonates (Appendices 6-8), while the amount is usually less than found in the pyrites it warrants further study to determine if there is an interference with Mg. The maximum observed As concentration in an arsenopyrite grain in the Cape Coral core occurred in CPS-4 835-835.5 ft BLS and equaled 41.5 percent, or 414,880 ppm in (Figures 8 and 16). It was the only such grain found and could possibility be detrital just as the ilmenite and rutile.

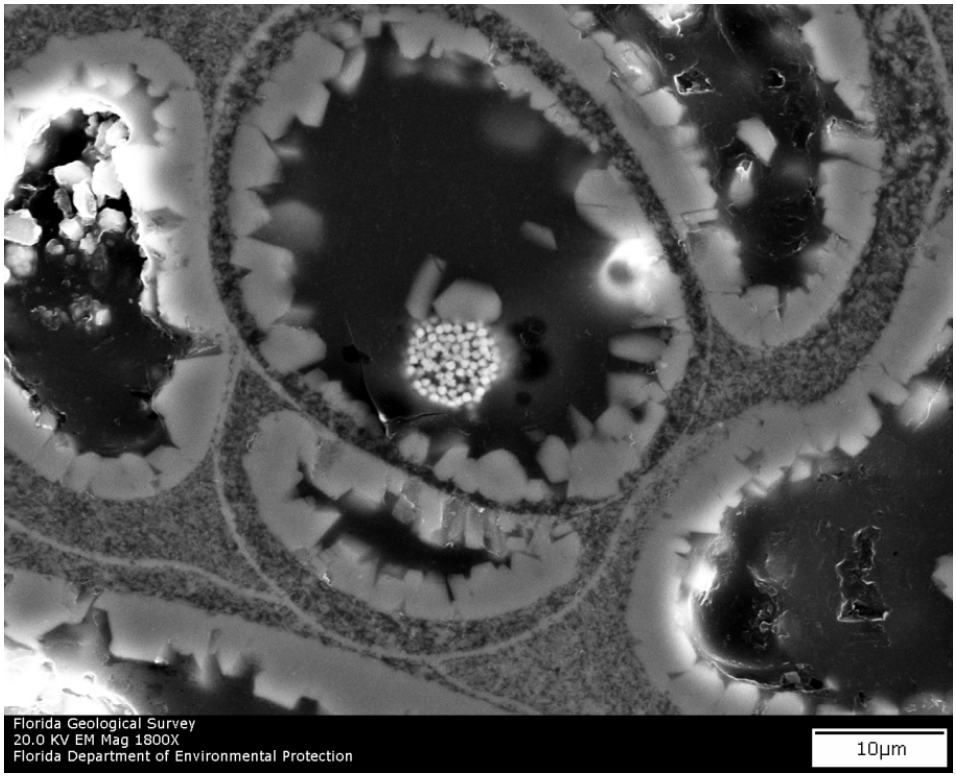

Figure 12. Secondary electron image (SEI) of pyrite framboid CPS-4 830.75-831 ft BLS.

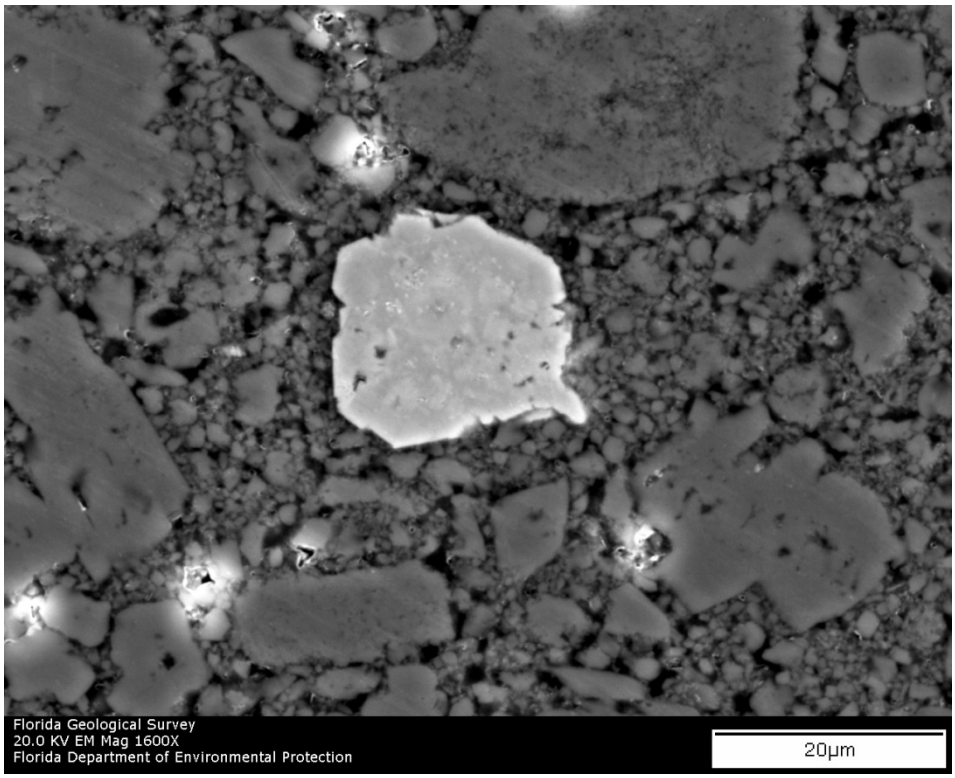

Figure 13. SEI of pyrite CPS-4 817-817.5 ft BLS.

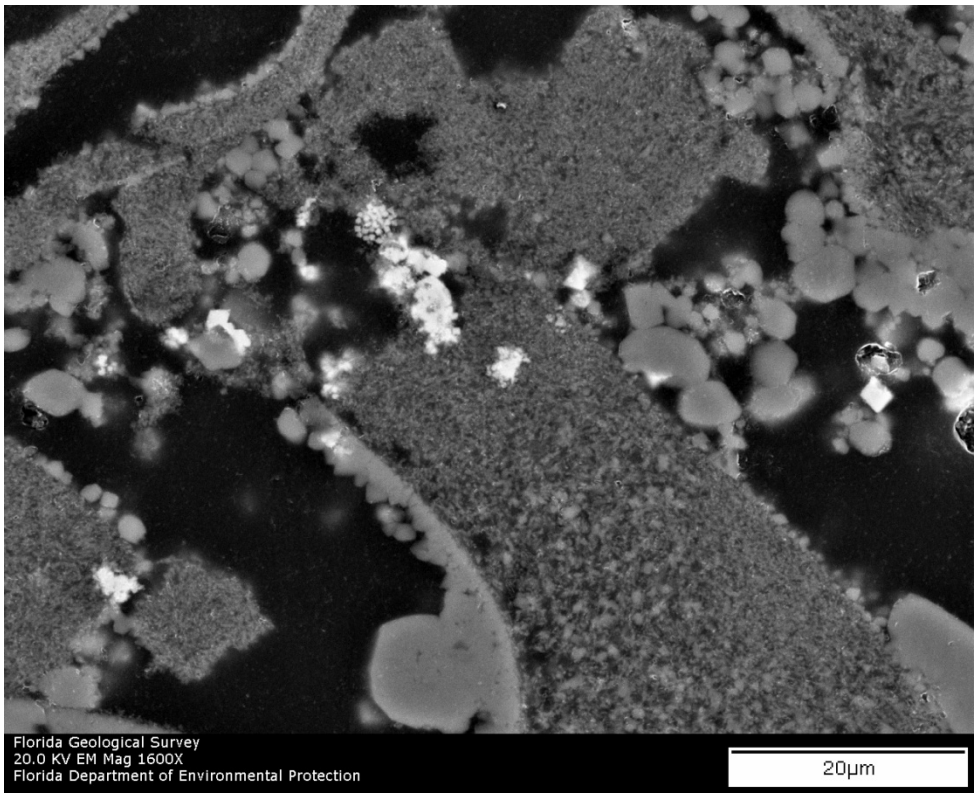

Figure 14. SEI of pyrite morphology-framboids, crystals, and clusters. CPS-4 at 847.5-848 ft BLS.

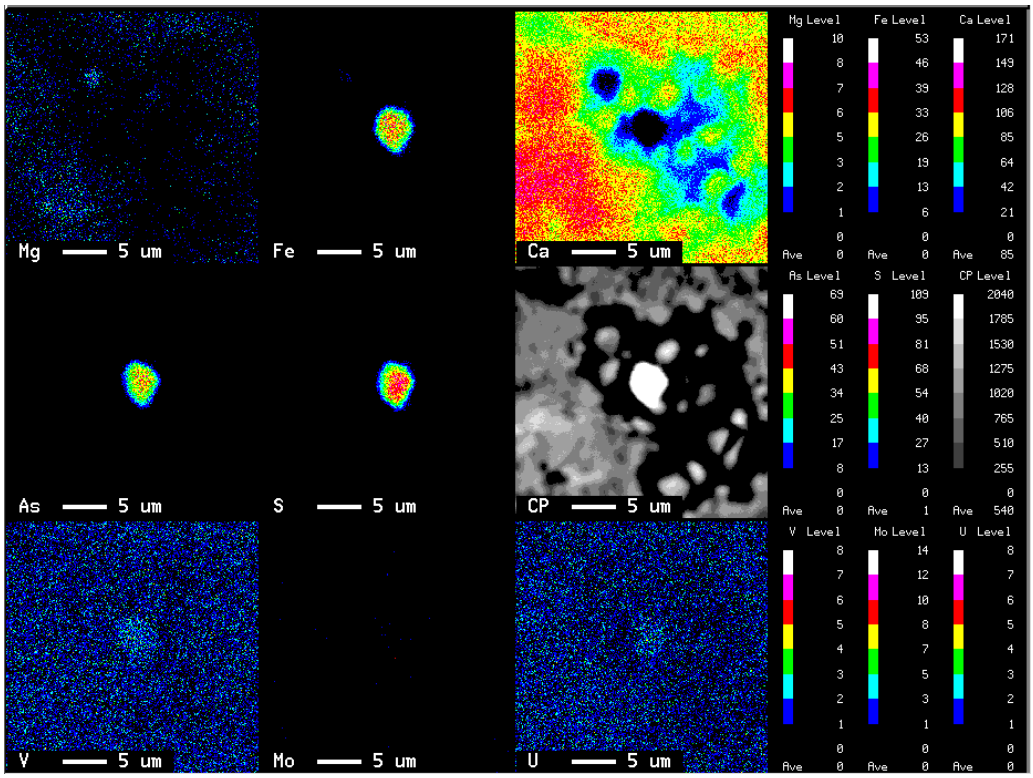

Figure 15. Element map (WDS) of arsenopyrite CPS-4 at 835-835.5 ft BLS. See also accompanying EDS spectrum (Figure 16).

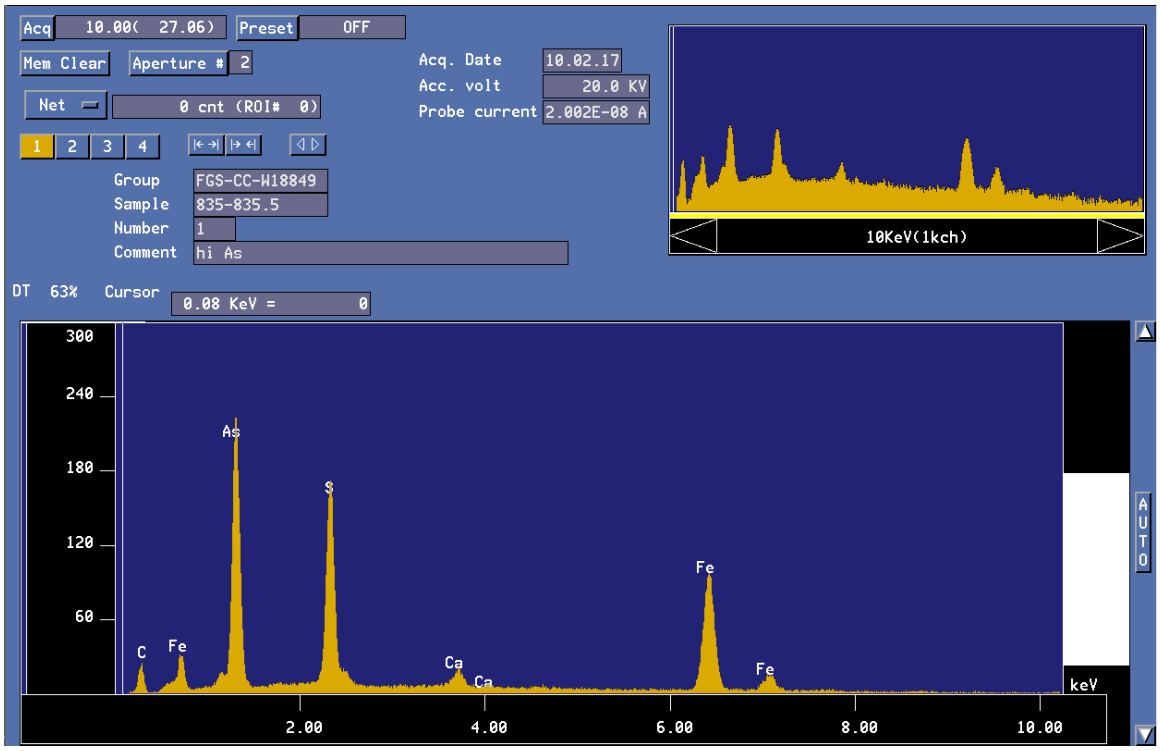

Figure 16. EDS spectrum of arsenopyrite (See also Figure 15).

Matrix Geochemistry

Whole-rock geochemical analyses are tabulated in Appendix 2. Table 7 contains a subset of the data in Appendix 2 to facilitate comparison of rock chemistry to trends in leachate chemistry as presented in charts later in this section.

Table 7. Selected lithogeochemical analyses of bench leaching samples.

		SiO2	Al2O3	Fe2O3(T)	MgO	CaO	Na2O	As	Mo	Ni	Sb	U	V
Well	Detection Limit	0.01	0.01	0.01	0.01	0.01	0.01	1	2	1	0.1	0.01	5
ID	Depth (feet BLS)	%	%	%	%	%	%	ppm	ppm	ppm	ppm	ppm	ppm
NSTS	840-841	0.82	0.15	0.1	0.42	55.49	0.05	BDL	BDL	2	0.1	3.24	11
NSTS	851.5-852.5	0.63	0.14	0.04	0.45	55.58	0.04	BDL	BDL	3	BDL	3.59	13
CPS-2	837.5-838.5	1.92	0.14	0.08	0.82	53.45	0.18	BDL	BDL	1	BDL	2.58	10
CPS-2	842.5-843	6.68	0.26	BDL	0.86	50.19	0.21	BDL	BDL	2	BDL	5.34	17
CPS-4	830-830.75	3.07	0.23	0.07	0.46	54.26	0.07	BDL	BDL	3	BDL	5.22	24
CPS-4	832-833	3.59	0.38	0.18	0.57	53.69	0.07	2	7	5	0.2	5.97	16
CPS-4	834-835	6.62	0.24	0.07	0.57	50.52	0.08	1	BDL	4	0.1	3.8	11

Bench-scale Leaching Experiments

Protocol 1: Native Groundwater / Source Water

Analytical results for Protocol 1 are given in Appendix 9, and time series plots of selected leachate measurements are given in Appendix 10. Results for the entire study are also available in electronic spreadsheet format (Appendices 9, 11 and 13).

Protocol 1 consisted of two phases (Table 4). During the first phase, core samples were exposed to native groundwater that had been adjusted to low redox levels (ORP of -260 to -250 mV, relative to our electrode) by brief bubbling with a N_2/H_2S gas mixture (95 percent/5 percent). A N_2 headspace was kept in the reaction vessel to minimize interference by atmospheric O_2 and to maintain low-ORP conditions. This preliminary phase (Phase I) lasted 15 days, and was intended both to assess the possible effects of hydrous ferric oxide (HFO) formed during core handling and to restore the core material to its native redox state prior to the onset of Phase II.

Arsenic (As) concentrations in the native groundwaters used as leachates for Phase I were low (<1 μg/L). During the phase, exposure of the low-ORP leachate to core material from wells NSTS (vessels 1 and 2) and CPS-4 (vessels 5, 6, 8, and 9) resulted in significant release of arsenic, with maximum concentrations of 20 to 200 μg/L (Figure 17, circles). In these vessels, release of As from core material was observed within 24 hours of exposure, and concentrations increased monotonically for 10-15 days, before beginning to stabilize. In contrast, vessels 3 and 4, which contained core from well CPS-2, released significantly less As during Phase 1 (Figure 17), with maximum leachate concentrations of 8-10 μg/L.

At the end of Phase I, the leachate was removed from the batch reactor and replaced with oxygenated "source water," i.e. the water intended for storage, thereby beginning Phase II. The purpose of this phase was to simulate possible geochemical reactions that could occur in the storage zone of the Cape Coral ASR site as a result of source water injection. During this phase, the head space in the reaction vessels was air, and no effort was made to regulate the ORP of the leachate. Prior to core exposure, source water arsenic concentrations were 2-3 μg/L. Relative to Phase I, exposure of the core material to oxic source water resulted in very little As release (Figure 17, triangles) and in all vessels, As concentrations were generally <5 μg/L. Although concentrations were relatively static in vessels containing core material from wells NSTS and CPS-4, concentrations fluctuated in vessels 3 and 4 (CPS-2), with highest concentrations of 5-10 μg/L at the beginning of the phase, lower concentrations during the middle of the phase (< 1 μg/L), and higher concentrations (3-7 μg/L) during the remainder of the phase.

If the mass of As initially present in the leachate is considered negligible, the total mass of arsenic (μg) in a vessel is equal to the mass of As initially present in the core material:

$$As_{(vessel)} = M_{(core)} \times [As]_{(core)}$$

where $M_{(core)}$ is the mass of core (nominally 300 g) and $[As]_{(core)}$ is the measured concentration of As in the core material, determined by whole rock analysis (Table 7). The mass of As present in the leachate (μg) at any time *t* is given by:

$$As_{(leach)} = [As]_{(leach)} \times 1\ L$$

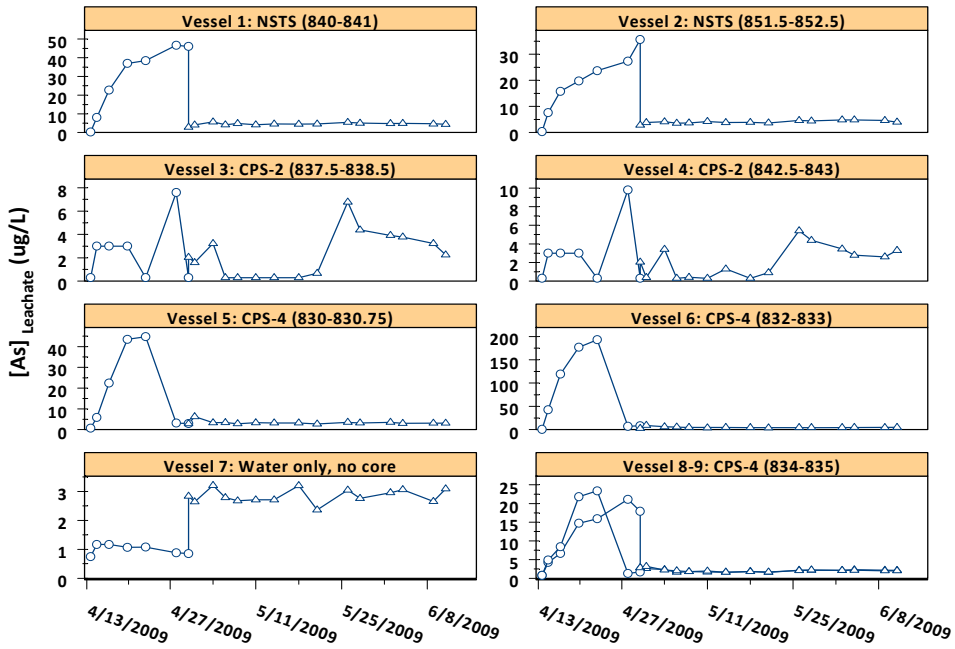

Figure 17. Arsenic leachate concentrations in batch reactors over time for Protocol 1. Open circles indicate Phase 1 results, while open triangles indicate Phase 2 results. Vessels 8-9 (lower right) each contained a split from the same core material. Note that vertical axis scale is unique to each plot.

where $[As]_{(leach)}$ is the measured concentration of As in the leachate at time *t* and 1 L is the volume of leachate in the reaction vessel. The fraction of As present in the leachate, i.e the fractional solubility, is then given by the quotient $As_{(leach)}/As_{(vessel)}$. Unfortunately, As concentrations were quantified in only two core samples (CPS-4 832-833 ft BLS, $[As]_{(core)}$ = 2 ppm; and CPS-4 834-835.5 ft BLS, $[As]_{(core)}$ = 1 ppm). Concentrations for the remaining core samples were below the detection threshold of 1 ppm. For these samples, substitution of the detection limit for $[As]_{(core)}$ may still be revealing since this will yield a minimum estimate of the leached fraction. Figure 18 shows these fractions over time for each of the 9 batch reactors. For vessels containing core material from wells NSTS (vessels 1 and 2) and CPS-4 (vessels 5, 6, 8, and 9), the percentage of As leached during Phase I ranged from 8 to 34 percent, while negligible fractions were released during Phase II. In vessels containing CPS-2 core (3&4), negligible fractions were released during both phases.

Leaching profiles for molybdenum (Mo) are shown in Figure 19. During Phase I, Mo leaching profiles closely resemble those for As, and maximum leachate concentrations in vessels 1, 2, 5, 6, 8, and 9 ranged from 85 to 1300 μg/L. The highest concentrations were seen in vessel 6 (CPS-4; 832-833 ft BLS), which also had the highest whole rock Mo concentration (7 ppm). However, unlike As profiles, Mo continued to be released during Phase II. In vessels 1, 2, and 6, Mo concentrations during the second phase were substantially lower than for the first phase. In vessel 5, concentrations in the second phase were nearly as high as in the first phase, while in vessel 9, Mo concentrations in both phases were approximately equal. Interestingly, in vessels 3 and 4, which showed little As evolved in either phase, Mo concentrations in the oxic phase were much higher than those observed during the anoxic phase.

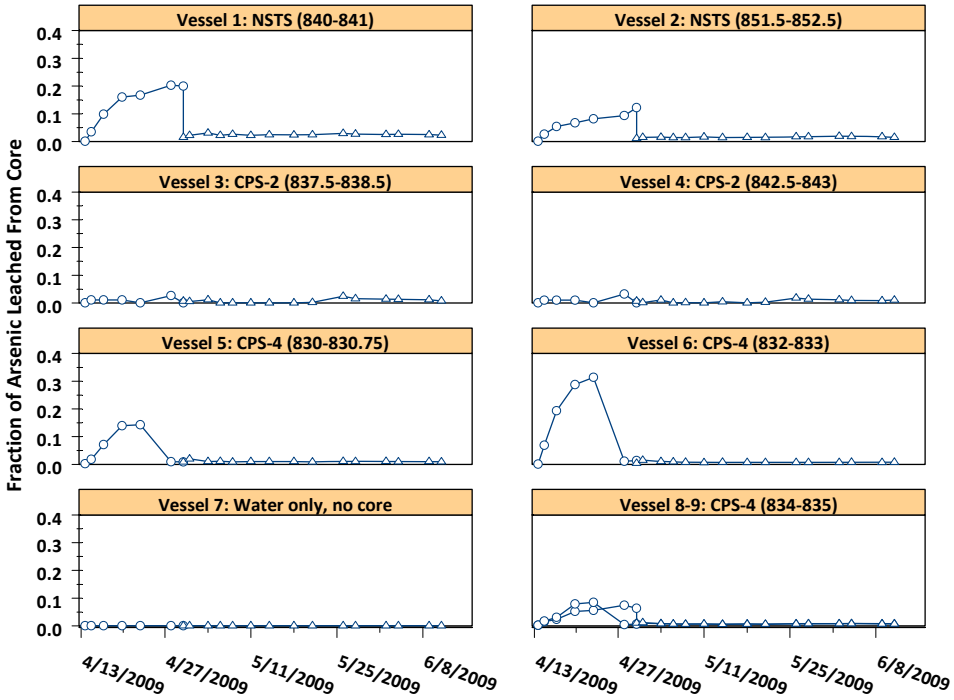

Figure 18. Fraction of arsenic leached from core material over time for Protocol 1. Open circles indicate Phase 1 results and open triangles indicate Phase 2 results.

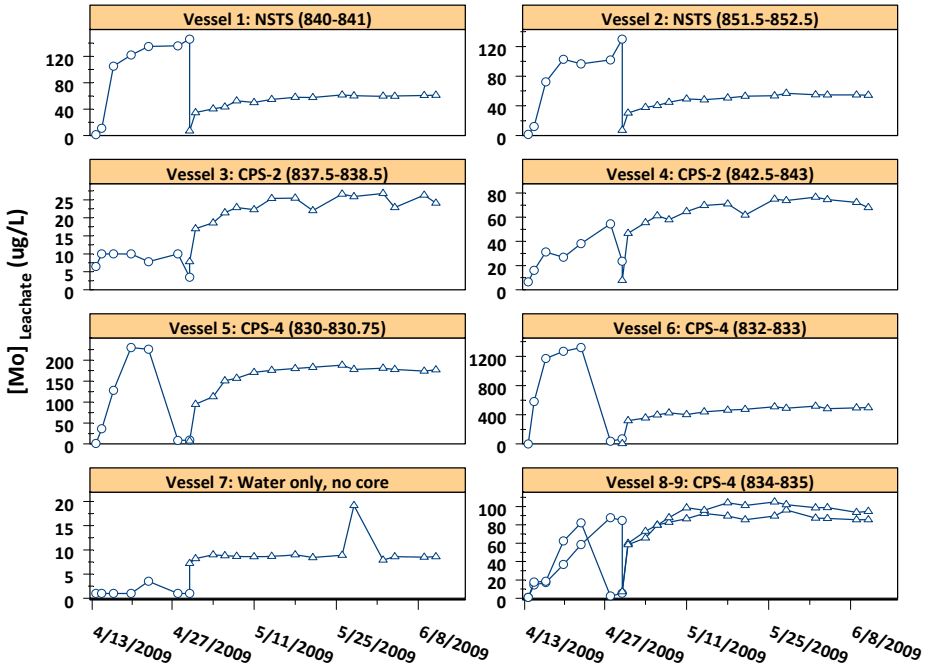

Figure 19. Molybdenum leachate concentrations in batch reactors over time for Protocol 1. Open circles indicate Phase1 results, while open triangles indicate Phase 2 results. Note that vertical axis scale is unique to each plot.

Leachate concentrations of Sb, though much lower than for As or Mo, nonetheless show distinctive changes over time (Figure 20). Concentrations were highest in vessel 6 (CPS-4) (maximum value was ~13 µg/L), which also had the highest whole rock Sb concentration (0.2 ppm). As with Mo, leaching of Sb was observed under both reducing (Phase I) and oxidizing (Phase II) conditions. Other trace metals showing distinctive trends include vanadium and thallium (mobilized during higher ORP conditions - Appendix 10, Figures 5 and 6) and uranium (mobilized during both phases - Appendix 10, Figure 7).

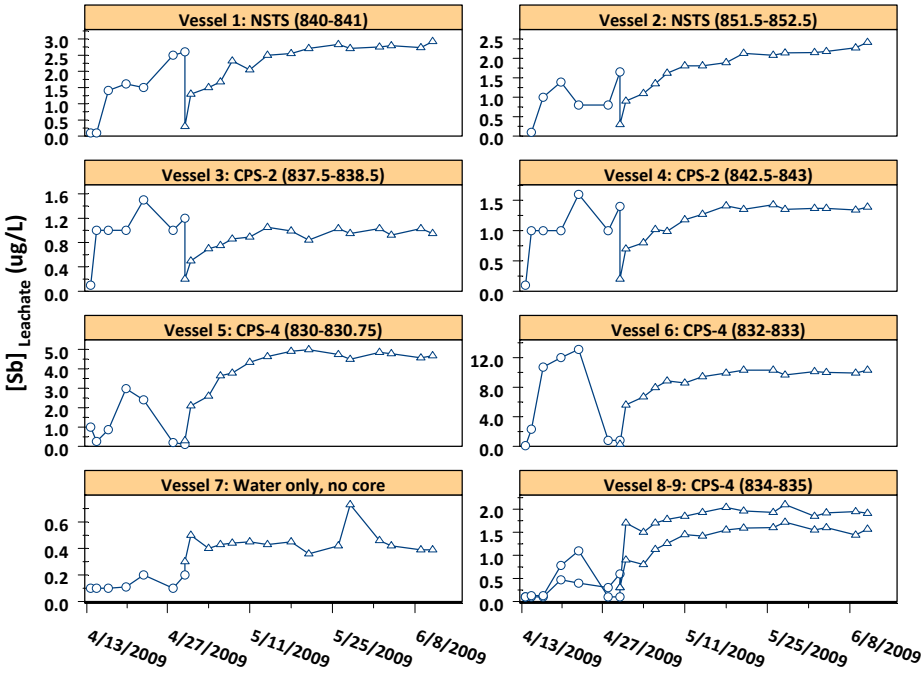

Figure 20. Antimony leachate concentrations in batch reactors over time. Open circles indicate Phase 1 results, while open triangles indicate Phase 2 results.

As discussed above, during Phase I an effort was made to maintain low redox conditions by filling the reaction vessel headspace with N_2 gas to minimize contamination by atmospheric O_2. Figure 21 shows ORP probe measurements over time, and indicates that a slow shift toward more oxidizing conditions occurred in most of the vessels during Phase I. Interestingly, the shift was most pronounced in the same vessels that showed the highest evolution of As (NSTS - vessels 1 and 2; CPS-4 - 5, 6, 8, and 9) while CPS-2 (vessels 3 and 4), which showed little As evolution, also showed little change in ORP. Because of increasing ORP values, the headspace in vessels 5, 6, and 9 was briefly replaced with the N_2/H_2S gas mixture (~20 sec) on 23-April, 2009, indicated in the plots by the red arrows. This lowered the ORP in the leachates to levels at or below the initial redox conditions, and at the same time greatly decreased the leachate concentrations of As, Mo, and Sb in these vessels (Figures 17, 19, and 20).

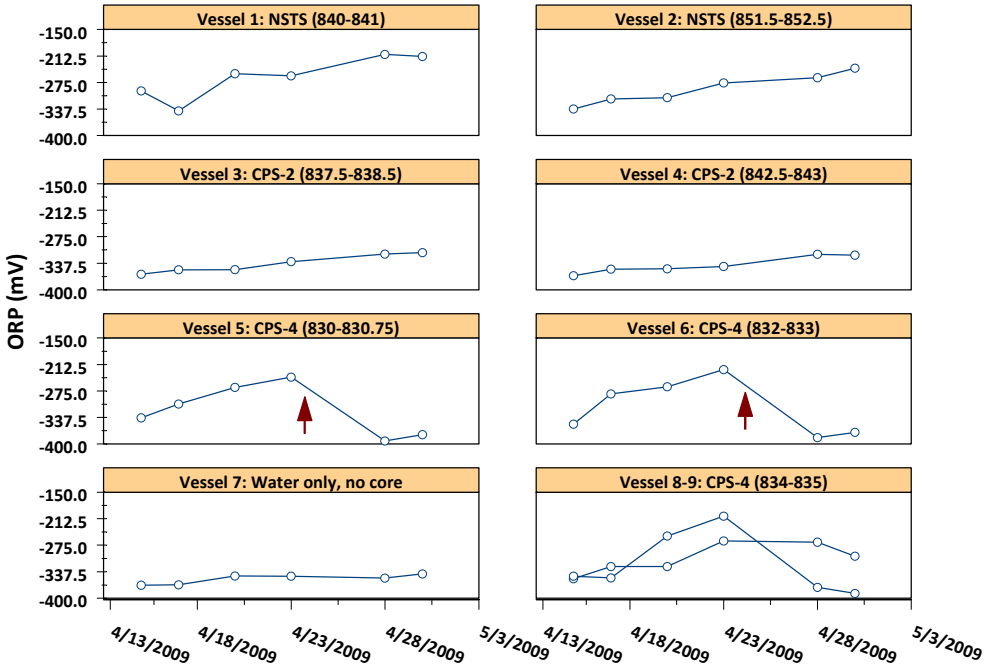

Figure 21. ORP values (relative to our electrode) in batch reactors over time for Phase 1, Protocol 1. Arrows in vessels 5-6 indicate re-exposure to N2/H2S to maintain low-ORP conditions.

Protocol 2: Deoxygenated Canal Water

Tabular results for Protocol 2 are given in Appendix 11, and time-series plots of selected leachate measurements are given in Appendix 12.

Protocol 2 included three phases (Table 5). In Phases I and II, leachate consisted of low-ORP (i.e. N_2/H_2S-sparged) source water. These phases were intended both to assess the effects of HFO formation during core handling and to restore the core material to its native redox state prior to the onset of Phase III. During Phase III, the leachate was source water (canal water) that had been deoxygenated using Liqui-Cel™ membrane contactors immediately prior to addition. The purpose of this last phase was to assess trace metal mobilization under anoxic, mildly reducing conditions.

Initial As concentrations in the source water leachates were low (1.5-3 μg/L), but increased over time with exposure to core until the time of the first water change (Figure 22-circles). In vessels 1 and 2 (NSTS), As levels reached 20-30 μg/L. Concentrations in vessels 5-8

(CPS-4) ranged from 14 to 90 µg/L, with highest concentrations in vessel 7. However, as with Protocol 1, core from well CPS-2 released very little As (Figure 22, vessels 3 and 4).

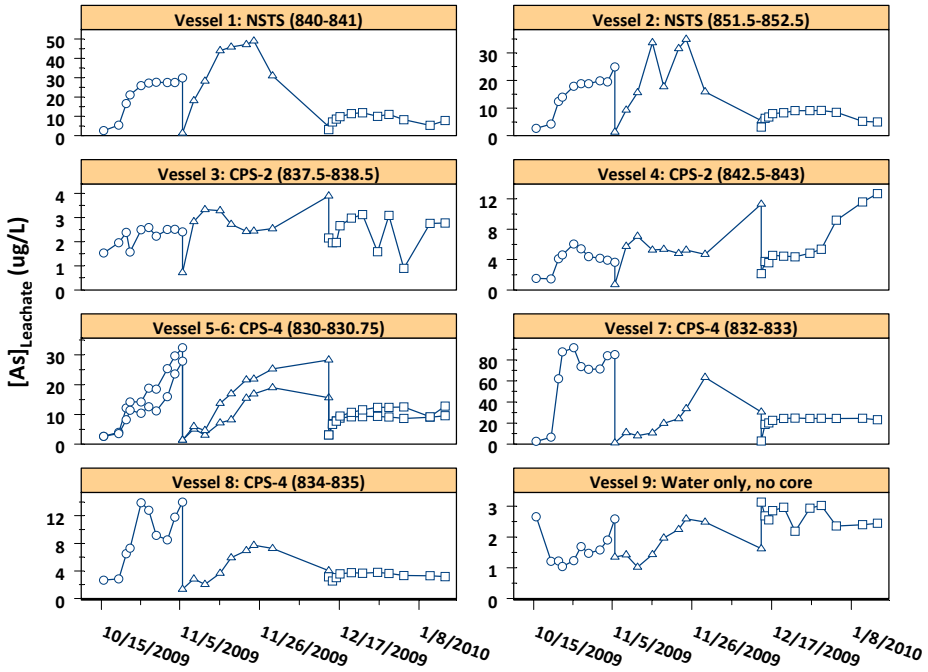

Figure 22. Arsenic leachate concentrations over time for Protocol 2. Open circles indicate Phase 1 results, open triangles indicate Phase 2 results, and open squares indicate Phase 3 results. Vessels 5-6 each contained a split from the same core material.

After the water change, arsenic continued to be released during Phase II, the second low-ORP phase (Figure 22- triangles). Concentrations in vessels 1 and 2 (NSTS) exceeded those observed during the first phase, by nearly twofold in vessel 1. The different leaching profiles observed in the first two phases of Protocol 1 and the first phase of Protocol I are likely related to the initial redox conditions or possibly to the initial H_2S concentration for individual vessels. This is discussed further in the next section. In vessels 5-8, As concentrations were 18 to 50 µg/L, while very low concentrations were again observed in vessels 3 and 4 (CPS-2). To maintain low redox conditions, the head space in vessels 1-4 were briefly filled with N_2/H_2S gas mixture on 30-Nov-2010, at which point As concentrations declined noticeably in vessels 1 and 2.

For Phase III, the leachate was changed to deoxygenated "Liqui-Cel" source water. DO levels are plotted against time in Figure 23. In vessels 4-9, DO levels were initially high (200-400 µg/L); however, after 48 hours, the range of DO for all vessels was between 110 and 180 µg/L. ORP values ranged from -310 to nearly 20 mV, and generally, either increased or were static during the phase (Figure 24). As concentrations, shown in Figure 22 (squares), were the lowest observed during Protocol 3, with maximum levels of 25 µg/L observed in vessel 7.

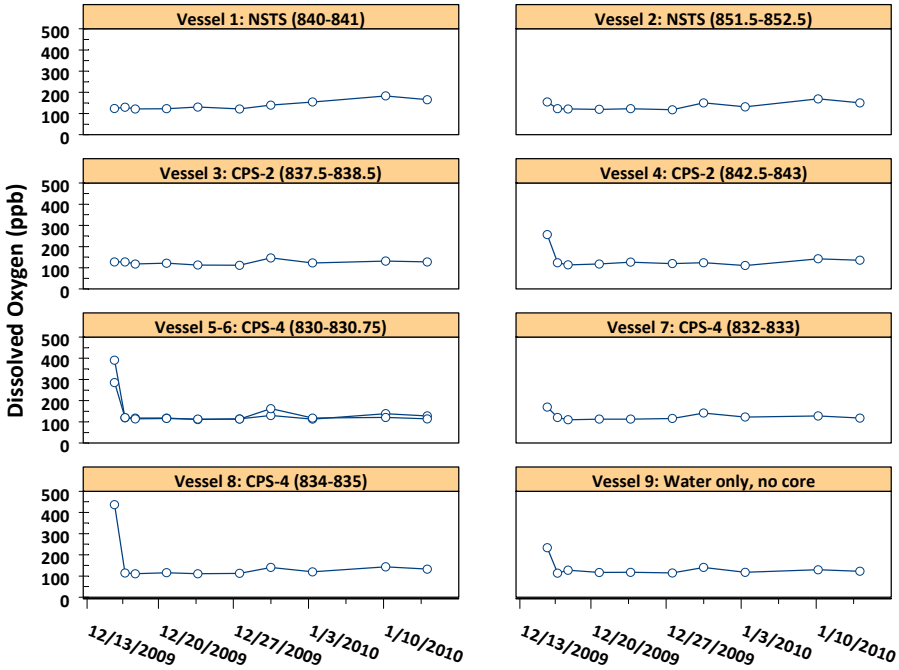

Figure 23. DO concentrations over time for Phase 3 of Protocol 2.

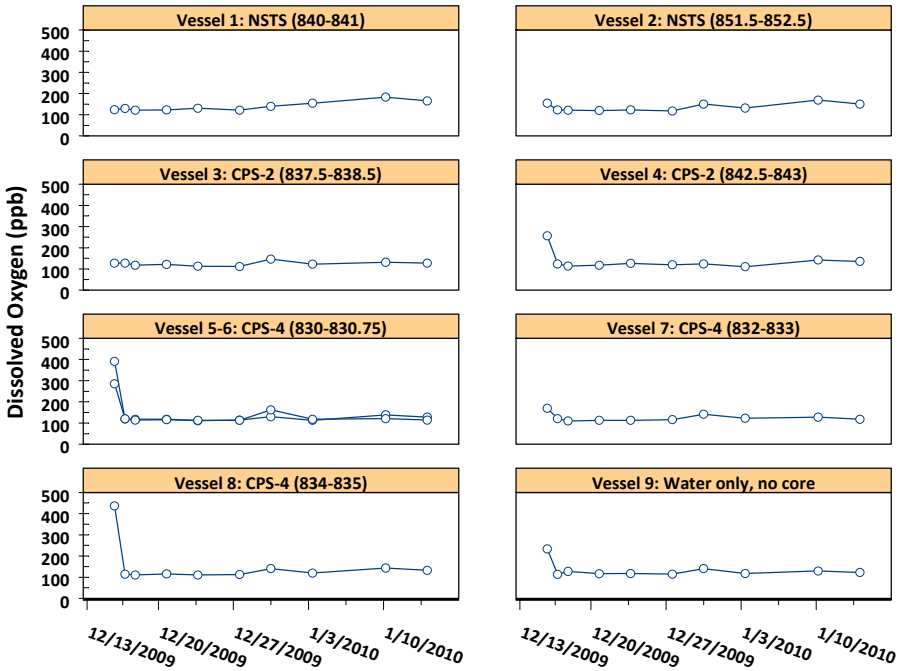

Figure 24. ORP values over time for Phase 3 of Protocol 2.

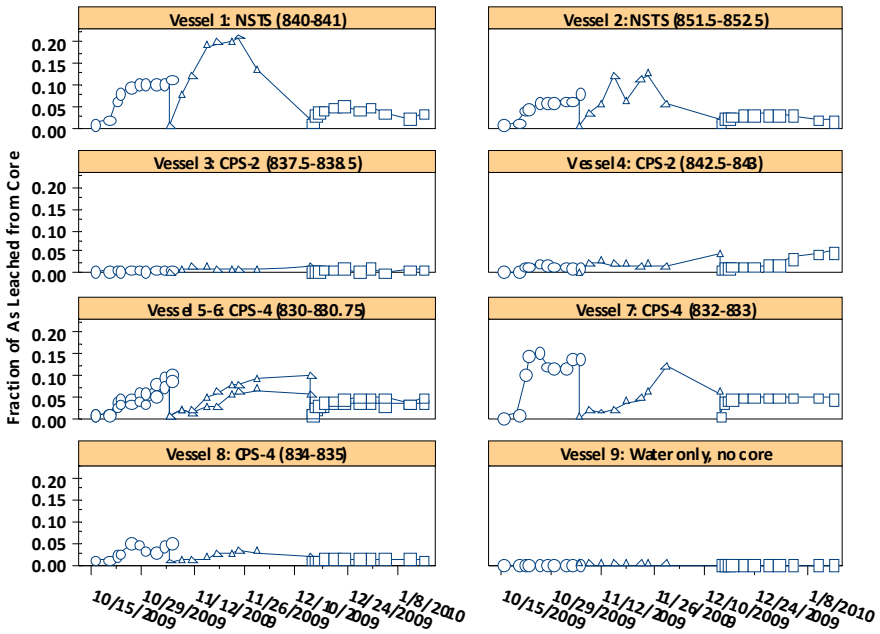

Figure 25. Fraction of arsenic leached from core material over time for Protocol 2. Open circles indicate Phase 1 results, open triangles indicate Phase 2 results and open squares are Phase 3 results.

Fractional solubilities for Protocol 2 are shown plotted against time in Figure 25. Minimum fractional solubilities ranged from 0.3 to 21 percent, and were highest in core samples NSTS 840-841 ft BLS (vessel 1, >21 percent) and CPS-4 832-833 ft BLS (vessel 7, 16 percent). For vessels 1 and 2, the fraction of As leached was greatest during the second phase, reflecting both the greater concentrations leached during the second phase, as well as the lower total mass of As in the vessels at the beginning of the phase. In the remaining vessels, the leached fractions were similar for Phases I and II. Fractional solubilities were lowest in Phase III, and were generally less than 5 percent.

Leaching profiles for Mo and Sb during Protocol 2 are shown in Figures 26 and 27. Maximum Mo leachate concentrations during Phase I ranged from 20 to 1200 μg/L, and a distinct concentration plateau was reached in most of the vessels by the middle of the phase. Unlike As, most of the Mo was leached during Phase I, and relatively little was leached during the second low-ORP phase, or during the deoxygenated water phase. Sb concentrations were much lower (0.6-15 μg/L), yet showed similar profiles during Phase I. However, unlike As and Mo, Sb leaching continued to occur during Phase II and Phase III. Vanadium and thallium, mobilized during the second phase of Protocol 1, showed little mobilization during Protocol 2 (Appendix 12, Figures 5 and 6). Mobilization of uranium was observed during Protocol 2, and appears to be less responsive to redox conditions than other metals.

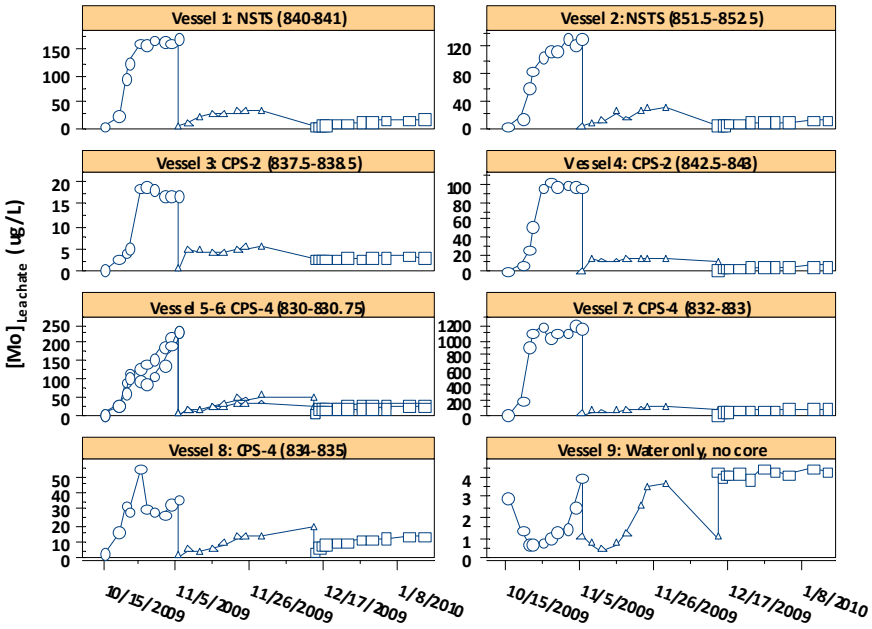

Figure 26. Molybdenum leachate concentrations over time for Protocol 2. Open circles indicate Phase 1 results, open triangles indicate Phase 2 results, and open squares indicate Phase 3 results.

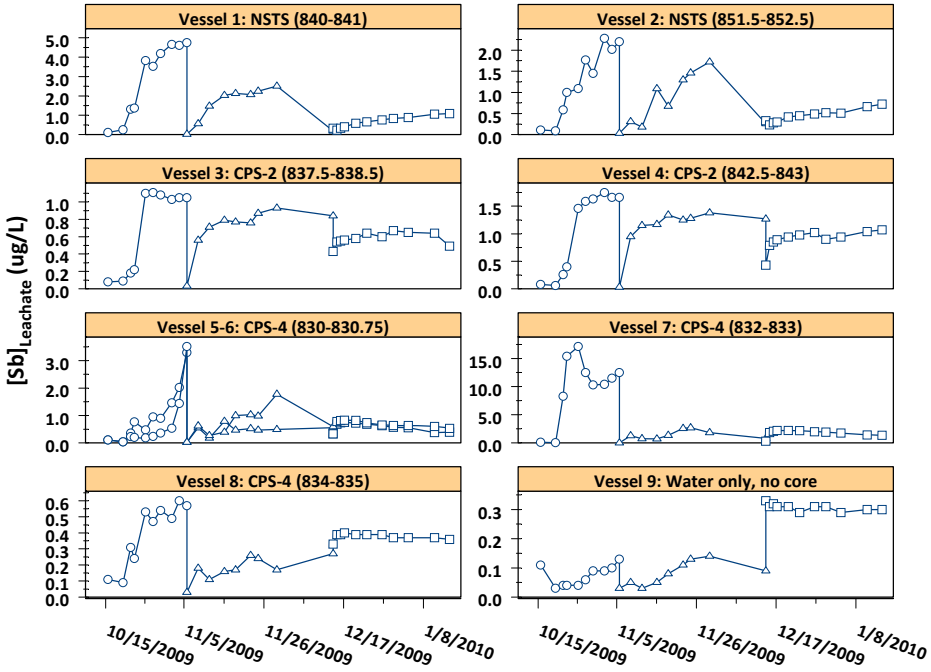

Figure 27. Antimony leachate concentrations over time for Protocol 2. Open circles indicate Phase 1 results, open triangles indicate Phase 2 results, and open squares indicate Phase 3 results.

Protocol 3: Hyperoxic to Oxic Canal Water

Results for Protocol 3 are given in tabular form (Appendix 13), and time-series plots of selected leachate measurements are given in Appendix 14.

Protocol 3 consisted of four leaching phases using oxygenated canal water (Table 6). The duration of each phase was approximately 21 days, with 8 to 9 samples collected per phase. The first 3 phases were conducted under supersaturated oxygen conditions (DO ≈ 20 mg/L), and the fourth phase under saturated conditions (DO ≈ 8 mg/L). DO levels were slightly lower than intended at the beginning of the hyperoxic phases because O_2 tended to degas from the oversaturated source water; however, levels quickly rose to the target concentration under the 1:1 N_2/O_2 headspace (Appendix 14; Figure 9).

Concentrations of As measured during this protocol ranged from 2 to 25 μg/L (Figure 28). Concentrations were typically highest during Phase I, and decreased with each successive phase. Concentrations were highest in vessel 6 and 7, which contained core CPS-4 (832-833 ft BLS). In vessels 1, 2, 5, 6, 7, 8, As typically reached maximum concentrations within 1-2 days. However, vessels 3 and 4 (CPS-2) show a dramatically different pattern in which As initially present in the source water was immediately removed from solution, remaining below the detection limit for several days, before reappearing in the leachate. This pattern was only observed during Phase I, and subsequent phases showed As levels at or just slightly above the initial leachate concentrations. The fraction of As in the leachates over the course of Protocol 3 was much lower than for the previous low-ORP protocols (0-4 percent, data not shown) and was equivalent to that observed during the deoxygenated source water phase of Protocol 2.

The concentration profile for Mo is shown in Figure 29. In contrast to As, high concentrations of Mo were liberated during Phase I of this protocol. Leaching of core NSTS (vessels 1 and 2) produced maximum Mo concentrations of 15-200 μg/L, while core CPS-4 produced maximum concentrations of 160-1600 μg/L. In each of the vessels, most of the Mo in the leachate was released within the first 24-48 hours of each phase, and subsequent phases showed decreasing Mo concentrations. Vessels 6 and 7 contained ~300 g of core CPS-4 832-833 ft BLS with Mo concentration of 7 μg/g, or approximately 2100 μg of Mo. Thus, approximately 76 percent of the total Mo present in the core was leached during Phase I. Integrating the maximum leachate concentrations from successive phases (~310, ~50, and ~20 μg/L for phases 2, 3, and 4, respectively) yields a total leachate of about 2000 μg, suggesting that nearly the entire available Mo was solubilized over the course of Protocol 3. U, Tl, and V, were also were readily solubilized (Appendix 14; Figures 5-7).

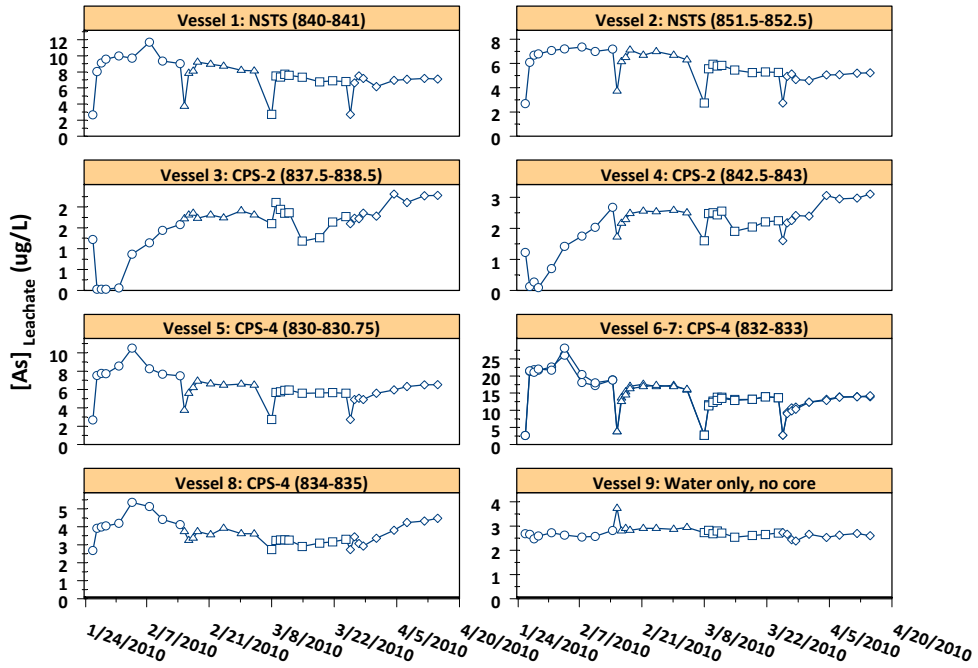

Figure 28. Arsenic leachate concentrations over time for Protocol 3. Open circles indicate Phase 1 results, open triangles indicate Phase 2 results, open squares indicate Phase 3 results, and open diamonds are Phase 4 results.

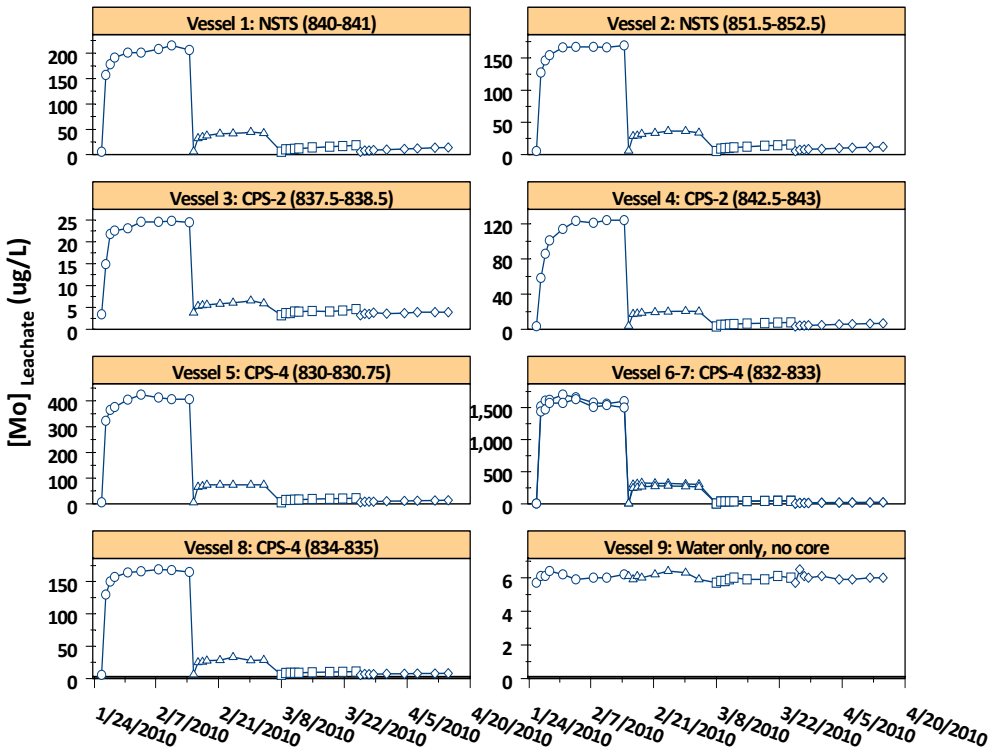

Figure 29. Molybdenum leachate concentrations over time for Protocol 2. Open circles indicate Phase 1 results, open triangles indicate Phase 2 results, open squares indicate Phase 3 results and open diamonds are Phase 4 results.

DISCUSSION

Mechanisms of Arsenic and Molybdenum Release

The goal of batch studies is to determine the conditions under which a particular metal mobilization mechanism might operate. Using this information, the character of the recharge water can be adjusted in such a way that release of arsenic and other undesirable metals can be minimized. Therefore, understanding the mechanisms operating in batch reactor experiments is critical. Appelo (2008) discussed three well-studied mechanisms for mobilization of As in groundwater systems. These include: reductive dissolution of hydrous ferric oxides (HFO), with consequent release of surface-sorbed As and other trace metals; oxidative dissolution of As-bearing pyrite; and release of surface-bound As during exchange reactions with bicarbonate and other anions. Recently, two specimens of the mineral powellite ($CaMoO_4$) were identified in core samples of the Suwannee Limestone. Because WDS analyses of these specimens revealed high levels of As associated with this mineral (~18,000 ppm), powellite dissolution has been proposed to represent an additional mechanism for As and Mo release (Pichler, 2010). Each of these mechanisms requires specific geochemical preconditions and each predicts specific outcomes. These are compiled in Table 8, and can be used to identify protocol/phase-specific mechanisms that might be operating during the batch experiments. In this section, the results from the various batch experiments will be discussed within this framework.

Pyrite Oxidation

As discussed above, pyrite was observed in most thin sections. Although pyrite concentrations in bulk rock samples were not quantified, they are constrained by both $[Fe]_{bulk}$ and $[S]_{bulk}$, such that maximum pyrite concentrations of 0.1 to 0.3 percent are indicated for most samples. Assuming the lower value, and assuming that As and Mo are primarily associated with pyrite, the bulk rock concentrations of these elements can be calculated based on their measured abundances in pyrite, determined by WDS to be ~0.13 and ~0.6 percent, respectively. These calculated bulk rock concentrations agree reasonably well with measured values, when concentrations were sufficiently high to be detected. Thus, the emphasis on pyrite oxidation as a likely release mechanism seems to be well justified. However, although the presence of As-bearing pyrite is a necessary condition for this mechanism, as shown in Table 8 (Reaction I) it is not alone sufficient. Other requirements were probably not met under all experimental conditions, and evolved leachate concentrations often did not agree well with those predicted from reaction stoichiometries.

For example, As reached its greatest concentrations during the low-ORP phases of Protocol 1 and Protocol 2 (Figures 17 and 22). However, it is unlikely that sufficient O_2 was available to oxidize the quantity of pyrite needed to account for the observed [As] and [Mo]. Each batch reactor contained ~300 g of core material; thus, if the pyrite content is assumed to be 0.1 percent, then approximately 2.5 mmol pyrite was present in each reactor. From the equation for pyrite oxidation shown in Table 8, oxidation of 2.5 mmol pyrite would consume ~ 5.6 mmol O_2, or about 180 mg (assuming that ~60 percent of the pyrite must be oxidized to order to account for the observed Mo concentrations). However, it is unlikely that this much O_2 was available. Measured O_2 concentrations were nearly always below 0.2 mg/L (the detection limit of our meter), and although it is expected that minor O_2 contamination may have occurred during the experiment, it would likely be insufficient to oxidize the requisite pyrite (e.g., this would require saturating the leachate with oxygen more than 20 times, which our measurements should have

Table 8. Arsenic Mobilization Methods.

Reaction I: Complete Pyrite Oxidation $As\text{-}FeS_2 + 15/4\ O_2 + 7/2\ H2O \rightarrow As\text{-}Fe(OH)_3 + 2\ SO_4^{2-} + 4\ H^+$

Necessary Conditions for Reaction	Expected Products of Reaction
1. Arsenian pyrite must be present. 2. Substantial oxygen must be available.	1. High concentrations of sulfate. 2. Decrease in pH if solution is not well buffered. 3. Minimal release of As due to resorption to HFO.

Reaction II: Partial Pyrite Oxidation $As\text{-}FeS_2 + 7/2\ O_2 + H_2O \rightarrow Fe^{2+} + As_i + 2\ SO4^{2-} + 2\ H^+$

Necessary Conditions for Reaction	Expected Products of Reaction
1. Arsenian pyrite must be present. 2. Some oxygen must be available.	1. High concentrations of dissolved iron. 2. Increased dissolved inorganic arsenic (As_i). 3. Decrease in pH in unbuffered solutions. 4. Significant increase in dissolved sulfate.

Reaction III: Reductive dissolution of HFO $As\text{-}FeOOH + CH_2O + 7H^+ \rightarrow Fe^{2+} + HCO_3^- + 6\ H_2O\ + As_i$

Necessary Conditions for Reaction	Expected Products of Reaction
1. HFO must be present. 2. Iron-reducing bacteria must be present. 3. No oxygen or nitrate should be available. 4. Must have oxidizable organic carbon.	1. Increase in alkalinity (may not be observable). 2. High concentrations of dissolved iron. 3. Liberation of inorganic arsenic.

Reaction IV: Anion exchange $AsO_4^{3-}\text{-}HFO + HCO_3^- \rightarrow HCO_3^-\text{-}HFO + AsO_4^{3-}$

Necessary Conditions for Reaction	Expected Products of Reaction
1. HFO or other sorbent must be present. 2. Exchanging anions (e.g. HCO_3^-, $H_2PO_4^-$).	1. Decrease in anions (may not be observable). 2. Liberation of inorganic arsenic.

Reaction V: Powellite dissolution $As\text{-}CaMoO_4(s) \rightarrow Ca^{2+} + MoO_4^{2-} + As_i$

Necessary Conditions for Reaction	Expected Products of Reaction
1. Powellite must be present. 2. Calcium should be initially low.	1. Increase in molybdate and inorganic arsenic concentration. 2. Increase in calcium concentration (may not be observable).

detected). Other studies have documented arsenic mobilization under similar conditions, ostensibly in the absence of O_2 (Arthur, et al., 2007c).

Also, pyrite oxidation should have greatly increased sulfate concentrations in the leachate. Continuing with the example above, oxidation of 1.5 mmol pyrite is predicted to produce 3.0 mmol sulfate; this would increase the leachate concentration by approximately 300 mg/L. During the first 48 hours of leaching sulfate concentrations did typically increase (for example, about 45 mg/L for CPS-4 832-832 ft); however, this is about one-sixth the predicted amount. Also, other reactions such as gypsum dissolution may have caused the observed sulfate increase. Gypsum dissolution should be marked by a concomitant increase in Ca concentration, which though observed, was not sufficient to account for the observed increase in sulfate. It is possible that the additional Ca was precipitated as $CaCO_3$, which would be consistent with the observed decreases in alkalinity observed during the course of these phases.

Finally, in contrast to our experimental observations, it has been suggested that As concentrations should not increase as a result of pyrite oxidation. As indicated in Table 8, complete oxidation of pyrite (mechanism 1) leads to HFO formation (e.g., ferrihydrite), yet because As has an extremely high affinity for HFO it is sequestered on these surfaces with little net transfer to solution (Appelo, 2008). When pyrite is partially oxidized (mechanism 2, Table 8), HFO is not produced; therefore, both Fe and As are expected to be released to solution in amounts proportional to their pyrite stoichiometry (approximately 500:1 by mass for $[As]_{pyrite}$ ~ 0.1 wt percent). In our experiments where Fe was released, the Fe:As ratio ranged from ~1 to 5, far below the expected value; thus evidence for this mechanism is also lacking.

Although pyrite oxidation in low-ORP experiments is not well-supported by our data, some caveats are appropriate. It is difficult to entirely exclude O_2 from batch experiments, and a small but constant flux of atmospheric O_2 into the headspace of the reactors could supply sufficient O_2 for pyrite oxidation. Also, although the expected concomitant increase in sulfate was not observed, partial oxidation of pyrite to solid hydrated ferrous sulfates (e.g. melanterite) could sequester both Fe and S in this metastable phase. Such a process might release Mo and As; however, it has not to our knowledge been reported in the literature. The fact that As evolution during the anoxic phases can be reasonably modeled as pyrite oxidation (Appendix 15) suggests that more work should be done to investigate the post-leaching mineralogy of the residual rock phase. Subject to these caveats, pyrite oxidation is not believed to be the dominant As release mechanism in the low-ORP phases.

Mo and As were also liberated in the supersaturated DO phases (Protocol 3, Figures 28 and 29). Approximately 1500 µg of Mo was leached from CPS-4 832-833 ft during the first phase, equal to about ~71 percent of the total Mo present in that core sample. For comparison, about 63 percent was leached during the first phase of Protocol 1. However, the profile for that phase shows a somewhat more gradual increase in [Mo], whereas Mo release during the hyperoxic phases appears to have occurred much more rapidly. Thus, it is not clear whether similar release mechanism(s) were operating.

In contrast to Mo, much less As was released during the hyperoxic phases (~4-5 percent) than during the sulfidic phases (30-35 percent). If during these phases As and Mo were released via pyrite oxidation, these differences could be attributed to preferential resorption of arsenite or arsenate, both of which have a greater affinity for HFO surfaces than the molybdate anion (Dzombak and Morel, 1990). It is interesting to note that similar to the Mo leaching profile, As evolution during the hyperoxic phase occurred rapidly, within the first 24 - 48 hours, relative to anoxic phases, under which it accumulated more slowly.

During the hyperoxic phases ample O_2 was available for complete oxidation of pyrite. However, as discussed above, pyrite oxidation sufficient to produce the observed Mo should have increased the concentration of SO_4^{2-} by approximately 300 mg/L. Similar to the anoxic phase, $[SO_4^{2-}]$ did increase, although much less than would be predicted for pyrite oxidation (e.g. ~35 mg/L for CPS-4 832-833 ft). Similar releases of Cl^- were also observed, primarily during the first phases of both protocols and within 24 hrs of core exposure. This suggests that these anions were perhaps being released by dissolution of salts formed as a result of pore-water evaporation that occurred during core drying, rather than by pyrite oxidation.

Reductive Dissolution of HFO

The WDS results showed significant As and Mo in association with pyrite, which combined with reasonable maximum estimates of the pyrite content, correspond well with the concentrations of As and Mo measured in the bulk rock. However, the true pyrite abundance in these samples may be less than these estimates if other solid phases containing Fe (e.g. HFO, glauconite, other clay minerals, etc) and S (organic matter, gypsum, anhydrite, etc) are present, as is likely. In this case, other As- and Mo-bearing phases must be present in order to account for the observed bulk rock concentrations.

HFO was identified in SEM images of some samples (Figure 9); however, a systematic or quantitative evaluation of HFO was not performed. In many samples, the $[Fe]_{bulk}$ is in excess of the amount predicted by the $[S]_{bulk}$, assuming $[S]_{bulk} = [S]_{pyrite}$ and this suggests the possibility that Fe phases other than pyrite might be present. These "excess iron" samples do not show an obvious pattern with depth, so it is possible that both HFO and pyrite coexist throughout the core (i.e., the bulk core is not in thermodynamic equilibrium). It is worth noting that for CPS-4, high $[As]_{bulk}$ and high $[Mo]_{bulk}$ were only found in samples with excess iron. These observations suggest that HFO may be present throughout the core and that it may constitute a complementary reservoir for As and Mo. Both As and Mo are known to sorb to HFO surfaces; therefore, dissolution of HFO has been proposed to liberate these metals (Pederson, et al., 2006).

Reductive dissolution of HFO (Reaction III, Table 8) occurs exclusively under anaerobic conditions; thus, with caveats noted above, this mechanism was possible only under low-ORP experiments with little O_2 (Phase 1 of Protocol 1, Phases 1 and 2, and possibly Phase 3 of Protocol 2). Iron-reducing bacteria, which oxidize organic carbon using Fe (III) as an electron acceptor, are naturally required. Although these bacteria were likely to have been present in the aquifer, their viability during core handling and storage was not assured, especially after drying of the core samples (CPS-4) in vacuum desiccators. Microbes may also have been present in the native groundwater and source water.

A necessary reactant for HFO reduction is organic carbon, the ultimate source of electrons used in iron reduction. Concentrations of organic carbon in most core samples were below the detection limit of 0.025 percent. However, several samples from core NSTS (W-18878) and one sample from CPS-4 (W-18849) were shown to have organic carbon at levels of 0.09 to 0.27 percent. It can probably be assumed that at least some organic carbon was present in most samples; however, its bioavailability, (i.e. the ease with which it can be respired by bacteria) is unknown. Unfortunately, the water used as leachates was not analyzed for organic carbon.

Reductive dissolution of HFO is predicted to mobilize Fe, because reduced Fe is quite soluble. In the first phase of Protocol 1, little dissolved Fe was detected in the leachates, possibly because the high ionic strength of the leaching solutions resulted in elevated detection limits. Fe concentrations increased dramatically, however, when the headspace was briefly filled with N_2/H_2S. It is speculated that the introduction of H_2S, which lowered the ORP to < -380 mV in some vessels, stimulated Fe reduction. This may have been due to direct abiotic reactions between H_2S and HFO, rather than microbially-mediated reduction. However, the introduction of sulfide caused immediate loss of As and Mo (Figure 30). This is perhaps due to the formation of thioarsenite and thiomolybdate complexes, which are believed to be largely insoluble under the conditions of our experiments. Precipitation of iron sulfides may also have occurred (some of the solutions turned cloudy), which may have co-precipitated Mo and As.

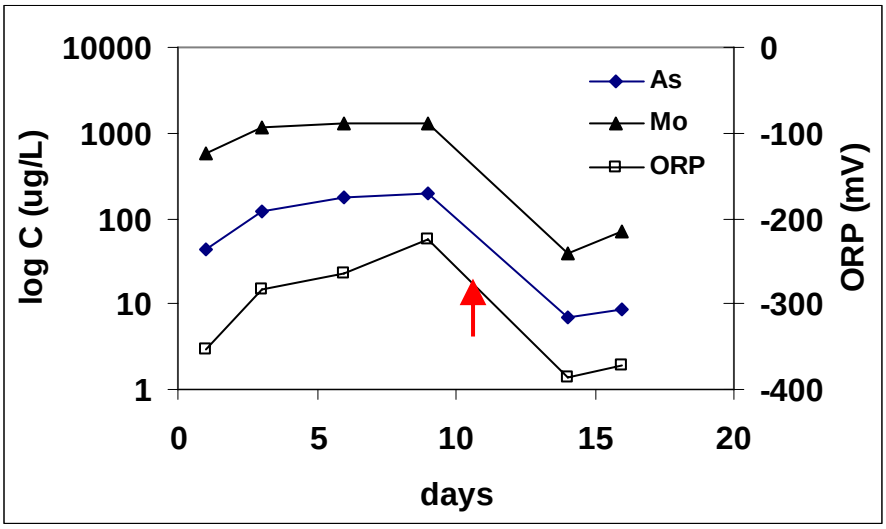

Figure 30. Log Mo concentration (triangles), log As concentrations (diamonds), and Eh (squares) over time for vessel 7 (W-18849) during Protocol 1, Phase 1. Re-sparging with N_2/H_2S at 11 days (red arrow) caused Eh and concentrations for both elements to decrease.

In contrast to Protocol 1, Fe was released in most of the batch reactors during the first phase of Protocol 2, consistent with HFO reduction (Figure 31). The source water used in this protocol was much lower in dissolved solids; and the resulting lower detection limits (10 µg/L) may account for the different observations. Also, canal water was the source of the leachates used in Protocol 2; consequently more organic carbon may have been available as a substrate for Fe reduction. Fe concentrations at the beginning of the phase were low, and reached maximum levels in the middle of the phase before declining again later in the phase. This Fe pattern may be related to increasing redox state (Figure 32). At low ORP, Fe leachate concentration was low. Peak Fe concentration corresponded to intermediate redox values, but decreased as the ORP increased further. This pattern was observed in several vessels, and could be the result of HFO reduction followed by re-precipitation as FeS. Additionally, the rate of HFO reduction will be related to microbial abundance, and increasing [Fe] is expected as the bacterial population increases (Pederson, et al., 2006).

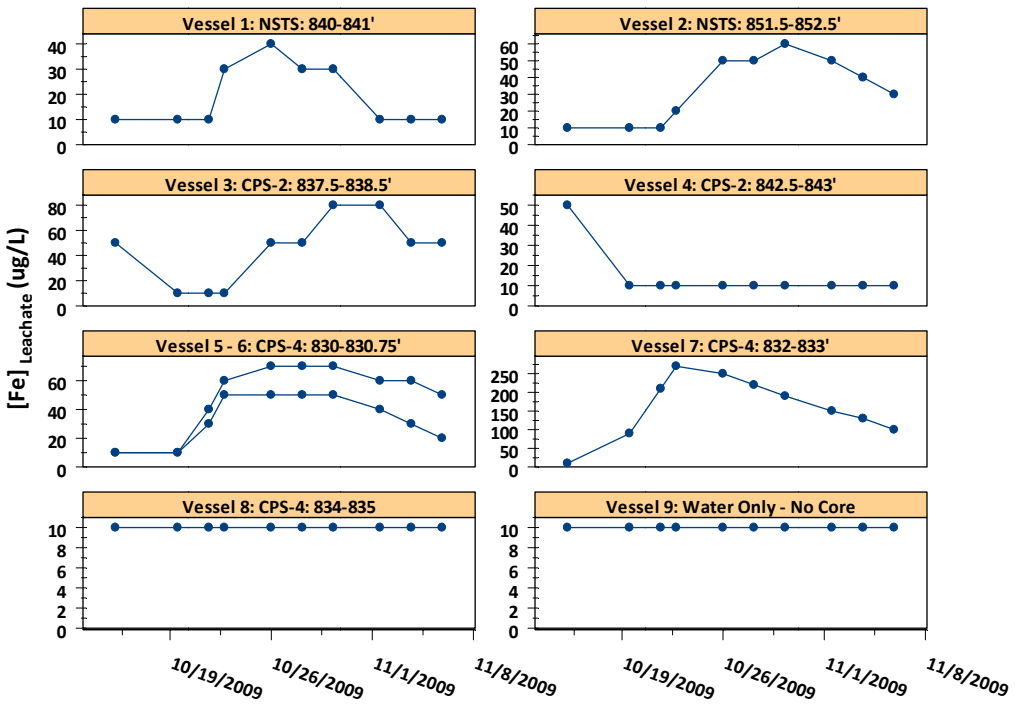

Figure 31. Fe concentrations during Protocol 2, Phase 1. Concentrations in vessel 8 and 9 were all below the detection limit (10 µg/L).

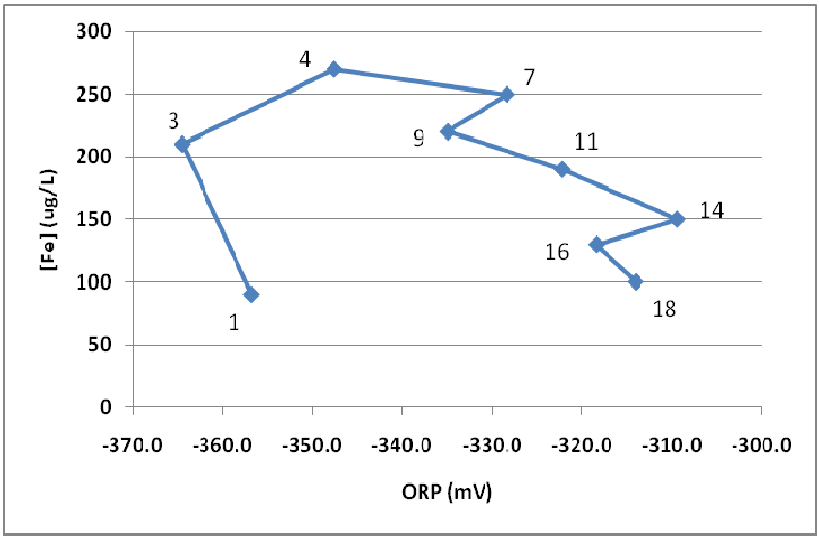

Figure 32. Fe versus ORP for Protocol 2 Phase 1 for CPS2 832-833 ft. (vessel 7). Labels are the number of days elapsed since the beginning of the phase.

The importance of HFO in these studies suggests the need to minimize any oxidation of pyrite that may occur during core collection and storage. Although preservation was attempted with one of the cores (CPS-4), controlled experiments to assess the effects of preservation were not performed. Anoxic leaching experiments under Protocol 1 showed that leaching of As, Mo, and Sb was greatest in core samples from this well, in spite of the fact that it was preserved. However, geochemical analyses later showed this core to contain the highest bulk concentrations of these metals; thus high leachate concentrations were to be expected. Controlled studies are currently underway to evaluate the effects of core handling on batch reactor experiments.

Summarizing, HFO reduction was theoretically possible in the low-ORP reduction phases of Protocol 1 (Phase 1) and Protocol 2 (Phases 1 and 2). HFO reduction is predicted to lead to the mobilization of Fe, as well as any sorbed impurities such as As and Mo. Mobilization of these metals was observed; however, additional research is needed to fully characterize the available carbon sources. Also, more analyses detailing mineralogical changes in the core material during the course of the leaching experiments would be useful.

Surface Exchange reactions

HFO (e.g. ferrihydrite) and iron sulfides (e.g. mackinawite, pyrite) have charged surfaces capable of sequestering arsenate, arsenite, molybdate and other anions. Although sorption of As and Mo to metal oxides has been well studied (Dixit and Hering, 2003; Xu, et al., 2006), these metalloids have been shown to sorb to iron sulfides as well (Bostick and Fendorf 2003; Wothers, et al., 2005; Xu, et al., 2006). Surface exchange reactions can result in net transfer of these sorbed oxyanions into solution, as more abundant anions such as bicarbonate and sulfate compete for sorption sites. An equilibrium state is eventually reached, determined by the relative concentrations and binding strengths of the competing ions, and by other variables, such as pH. For an aquifer already in equilibrium, a perturbation in one of these variables can stimulate a net release of the sorbed ions. For example, large increases in pore water bicarbonate concentration have been shown to displace arsenate, arsenite, or other sorbed anions from HFO surfaces (Anawar, et al., 2004), releasing these metal oxyanions into solution until a new equilibrium is reached. The consequent reductions in bicarbonate or sulfate may not be observed, since their concentrations are often several orders of magnitude greater than typical arsenic or molybdenum concentrations. Thus, inferring surface exchange solely on the basis of changes in water chemistry is not always possible.

Conditions for exchange reactions are expected to differ greatly between batch experiments and field studies. In particular, crushing of core material greatly increases the amount of surface area exposed to leaching. Furthermore, most of the newly exposed surface area is relatively "unweathered," i.e., it was not part of the mobile or effective porosity present under *in situ* conditions (Appelo, 2008). These surfaces will therefore be out of equilibrium with any solution to which they are exposed, including the native groundwater used in Protocol 1; correspondingly, surface exchange is likely to occur. Such surface exchange reactions could account for the relatively rapid leaching we observed under the various protocols/phases. In particular, the redox-independent leaching profile observed for Mo is suggestive of single process. Given that the WDS data indicate a strong relationship between Mo, As and pyrite, and lacking indications of significant pyrite oxidation (e.g. sulfate production), exchange reactions involving pyrite offer the best explanation for the observed leaching profiles.

It is difficult to quantify the relative contributions of these different processes to the overall leaching profiles obtained in this study. Presumably, to some degree all processes are

acting simultaneously to produce a net leaching profile. However, surface exchange reactions, the rates of which may have been greatly enhanced by core crushing, may be dominating the analytical signal, possibly swamping the contributions of other reactions. If this proves to be the case, then the extent to which the batch experiments approximate ASR field activities is limited. Future studies should consider incorporating column experiments (with minimal core disturbance) in tandem with batch reactor experiments so that surface area effects can be more carefully evaluated. Also, surface exchange reactions should be incorporated into modeling efforts to describe leachate evolution.

Powellite Dissolution

Recently, the mineral powellite was observed during SEM analyses of core samples collected from the Hawthorn Group (Pichler, 2010). Powellite ($CaMoO_4$), which has not been previously described in Florida, is considered to be an uncommon secondary mineral, primarily found in solid solution with scheelite ($CaWO_4$) (Hsu and Galli, 1973). WDS analysis of the powellite crystals indicated As as an impurity, at levels as high as 1.8 percent. It was proposed that powellite could be a geogenic source of Mo and As, which both occur at high concentrations in some wells near the town of Lithia. The presence of trace amounts of this mineral would generate high concentrations of Mo and As upon dissolution. For example, <0.002 percent powellite could account for the entire Mo present in CPS-4 832-833 ft (7 ppm bulk rock concentration). Under sulfidic conditions, Mo released from powellite dissolution would likely be rapidly re-precipitated as MoS_2. Under mildly reducing conditions both Mo and As would remain in solution, and under oxic conditions in the presence of HFO, Mo could remain in solution, as it would be out-competed for sorption sites by other anions present in solution. These predictions more or less fit our observations; however, powellite was not observed in our detailed studies of Cape Coral core material. Detection of a mineral present in such small quantities is highly unlikely, even with the most sophisticated analytical tools. Furthermore, given the high subsurface Mo concentrations present in the vicinity of the Lithia cores, it is possible that the specimens observed in the core samples were precipitated during core drying. Although the role of powellite in affecting groundwater sources in Florida remains quite tentative, its potential as a geogenic source of Mo and As will need to be considered in future studies.

CONCLUSIONS

Although As evolution was observed in all leaching experiments, clear differences were observed. Low-ORP (-200 – 350 mV) solutions leached more As than any of the other batch experiments, up to 35 of the total As present in the core samples. However, very low-ORP sulfidic conditions, induced by re-exposure to H_2S gas, immediately decreased these concentrations. ASR cycle testing using sulfidic source water is currently underway, and initial reports indicate some success at reducing As mobilization during storage (Pearce and Waldron 2010). Our findings suggest this may prove to be an effective approach in some storage zones.

The low-DO experiments using Liqui-cel water also leached As, but at much lower concentrations. In the hyperoxic experiments As was also leached but at concentrations much lower than those observed under the low-ORP conditions, presumably due to re-sequestration of As on HFO surfaces. Successive exposures to hyperoxic water resulted in attenuated responses, similar to those observed in ASR field tests, as As was repeatedly mobilized and removed.

The results of this study suggest that the applicability of bench-scale studies to real-scale processes can be improved. First, the importance of core preservation cannot be over emphasized. Although the design of these experiments did not allow for direct comparison of preserved versus unpreserved core (because the cores were different), studies currently in progress suggest that core handling may have an impact on these studies. Second, column studies conducted in parallel with batch studies might assist in identifying procedural influences, inherent in both approaches, on mobilization mechanisms. Finally, more quantitative information on pre-leaching and post-leaching mineralogy and trace element distribution would help to constrain model assumptions.

REFERENCES

Anawar, H.M., Akai, J., and Sakugawa, H., 2004, Mobilization of arsenic from subsurface sediments by effect of bicarbonate ions in groundwater: Chemosphere, v. 54: p. 753-762.

Appelo, C. A. J., 2008, Geochemical experimentation and modeling are tools for understanding the origin of arsenic in groundwater in Bangladesh and elsewhere, *in* Appelo, C.A.J., ed., Arsenic in groundwater: a world problem: Proceedings Seminar Utrecht, p. 33-50.

Arthur, J.D., Dabous, A.A., and Cowart, J.B., 2002, Mobilization of arsenic and other trace elements during aquifer storage and recovery, southwest Florida: U.S. Geological Survey Open-File Report 02-89, p. 47-50.

Arthur, J.D., Dabous, A.A., and Cowart, J.B., 2005, Chapter 24: Water-rock geochemical considerations for aquifer storage and recovery: Florida case studies, *in* Tsang, C.F., et al., eds., Underground Injection Science and Technology: Developments in Water Science Amsterdam, Elsevier, v. 52, p. 327-339.

Arthur, J.D., and Dabous, A.A., 2007, (in preparation) Bench Scale Geochemical Assessment of Water-Rock Interactions: Seminole County ASR Core Samples: Florida Geological Survey Open File Report, 95 p.

Arthur, J.D., Dabous, A.A., and Fischler, C., 2007a, (in preparation) Bench Scale Geochemical Assessment of Water-Rock Interactions: Sanford ASR Core Samples: Florida Geological Survey Report of Investigation 106, 112 p.

Arthur, J.D., Fischler, C., Dabous, A.A., Budd, D.A., and Katz, B.G., 2007b, (in preparation) Geochemical and mineralogical characterization of potential aquifer storage and recovery storage zones in the Floridan aquifer system, Comprehensive Everglades Restoration Plan: Final Report to the South Florida Water Management District for the ASR Regional Study.

Arthur, J.D., Dabous, A.A., and Fischler, C., 2007c, Aquifer Storage and Recovery in Florida: Geochemical Assessment of Potential Storage Zones, *in* Fox, P., ed., Management of Aquifer Recharge for Sustainability: Phoenix, Acacia Publishing, p. 185-197.

Arthur, J.D., Fischler, C., and Dabous, A.A., 2008, Bench-scale geochemical assessment of water-rock interactions: Orange County Aquifer Storage and Recovery Facility: Final Report to St. Johns River Water Management District and Barnes, Ferland and Associates, Inc., 42 p.

Bethke, M.C, 2008, Geochemical and Biogeochemical Reaction Modeling, 2nd ed.:New York, Cambridge University Press, United Kingdom, 543 p.

Bostick, B.C., and Fendorf, S., 2003, Arsenite sorption on troilite (FeS) and pyrite (FeS2): Geochimica Cosmochimica Acta, v. 67, p. 909-921.

Craw, D., Falconer, D., and Youngson, J.H., 2003, Environmental arsenopyrite stability and dissolution: theory, experiment, and field observations, Chemical Geology, v. 199, p. 71-72.

de Ruiter, H., and Stuyfzand, P.J., 1998, An Experiment on well Recharge of Oxic Water into an Anoxic Aquifer, *in* Peters, J.H., ed., Artificial Recharge of Groundwater: Nieuwegein, Netherlands, p. 299-304.

Dixit, S., and Hering, J.G., 2003, Comparison of arsenic (V) and arsenic (III) sorption onto iron oxide minerals: implications for arsenic mobility: Environmental Science and Technology, v. 37, p. 4182-4189.

Dzombak, D.A., and Morel, F.M.M., 1990, Surface complexation modeling: hydrous ferric oxide: New York, John Wiley and Sons, 393 p.

Hoffman, E.L., 1992, Instrumental Neutron Activation in Geoanalysis: Journal of Geochemical Exploration, v. 44, p. 297-319.

Hsu, L.C., and Galli, P.E., 1973, Origin of the scheelite-powellite series of minerals: Economic Geology, v. 68, p. 681-696.

Jones, G.W., and Pichler, T., 2007, Relationship between pyrite stability and arsenic mobility during aquifer storage and recovery in southwest central Florida, Environmental Science Technology, v. 41, p. 723-730.

Mindat.org: The mineral and locality database: www.mindat.org, mindat.org: (accessed August 2010)

MWH, City of Cape Coral, 2009, W-2C ASR well construction: North-south transfer station ASR well system completion report, 60 p.

MWH, City of Cape Coral, 2010, W-2C ASR well construction: Southwest Cape Coral water quality evaluation and monitor well completion report, 53 p.

Nordstrom, D.K., and Archer, D. G., 2003, in Arsenic in Groundwater, Welch, A. H. & Stollenwerk, K. G. eds., Boston, Kluwer, p. 1–25.

Pearce, M., and Waldron, M., 2010, The installation and performance of an ASR-water deoxygenation system developed for the SJRWMD and City of Deland using sodium bisulfide, *in* Proceedings of the American Institute of Professional Geologists/American Ground Water Trust, Annual Meeting, September, Orlando, 2010, p. 30-31.

Pederson, H.D., Postma, D., and Jakobsen, R., 2006, Release of arsenic associated with the reduction and transformation of iron oxides: Geochimica Cosmochimica Acta, v. 70, p. 4116-4129.

Pichler, T., Arthur, J., Price, R., and Jones, G., 2004, The arsenic problem during aquifer storage and recovery (ASR): 2004 Goldschmidt Geochemistry conference: Processes in Geochemistry, Forces, Fluxes, and Structure; Copenhagen, Denmark.

Pichler, T., 2010, Evaluating elevated arsenic and molybdenum concentrations at the Pritcher Road site, Lithia, central Florida: A final report prepared for the Florida Department of Environmental Protection, 75 p.

Pokrovski, G.S., Kara, S., and Roux, J., 2002, Stability and solubility of arsenopyrite, FeAsS, in crustal fluids. Geochimica et Cosmochimica Acta v. 66, p. 2361-2378.

Shock, E.L., and Helgeson, H.C., 1988, Calculation of the thermodynamic and transport properties of aqueous species at high pressure and temperature: correlation algorithm for ionic species and equation of state predictions to 5 kb and 1000°C.: Geochimica et Cosmochimica Acta v. 52, p. 2009-2036.

Wolthers, M., Charlet, L., van Der Weijden, C. H., Van Der Linde, P.R., and Rickard, D, 2005, Arsenic mobility in the ambient sulfidic environment: sorption of arsenic (V) and arsenic (III) onto disordered mackinawite: Geochimica et Cosmochimica Acta, v. 69, p. 3483-3492.

Xu, N., Christodoulatos, C., and Braida, W., 2006, Adsorption of molybdate and tetrathiomolybdate onto pyrite and goethite: effect of pH and competitive anions: Chemosphere, v. 62, p. 1726-1735.